TABLE 1. Comparisons of the Choroidal Thickness and Volume Between Healthy Pediatric and Adult Individuals

| | Pediatric Individuals | Adult Individuals | *P* Value |
|---|---|---|---|
| Eyes, *n* | 100 | 83 | |
| Mean age, y | 7.9 ± 3.1 | 54.5 ± 19.3 | <0.0001 |
| Mean axial length, mm | 23.13 ± 1.37 | 24.14 ± 1.17 | <0.0001 |
| Mean refractive error, D | −0.04 ± 1.96 | −0.25 ± 2.42 | 0.5256 |
| Central choroidal thickness, 1.0-mm circle, μm | 260.4 ± 57.2 | 206.1 ± 72.5 | <0.0001 |
| Macular choroidal thickness, 3.0-mm circle, μm | 255.2 ± 52.3 | 201.8 ± 68.6 | <0.0001 |
| Macular choroidal thickness, 6.0-mm circle, μm | 240.3 ± 45.6 | 190.8 ± 63.2 | <0.0001 |
| Central choroidal volume, 1.0-mm circle, $mm^3$ | 0.205 ± 0.045 | 0.160 ± 0.056 | <0.0001 |

quadrants. The individual sectors are referred to as the central, inner temporal, inner superior, inner inferior, inner nasal, outer temporal, outer superior, outer inferior, and outer nasal sectors. In addition, the macular choroidal thickness within a circle of 3.0- or 6.0-mm diameter, and within an inner or outer ring was calculated. Based on the choroidal thicknesses obtained, we calculated the choroidal volume for each sector of the ETDRS grid.

### Measurement of Reproducibility

Because the segmentation was done manually in some images, we evaluated the interobserver reproducibility of the corrections. The chorioscleral border in the OCT images of one raster scan was adjusted by two observers in 14 selected pediatric individuals before the study.[15] The thickness maps and mean choroidal thicknesses were calculated independently, and the intraclass correlation coefficient (ICC) for each ETDRS sector was calculated.

In addition, the methods described by Bland and Altman[28] was used to evaluate interobserver reproducibility.[29] The mean difference between two choroidal thickness measurements (Observer 1 − Observer 2) for each of the 14 individuals represented the bias. The 95% limits of agreement (LoA), the expected difference between two measurements, were calculated as the mean of the differences ± 1.96 × SD of the differences.

### Statistical Analyses

Student's *t*-tests were used to determine the significance of the differences in the age, axial length, refractive errors, central or macular choroidal thickness, and central choroidal volume between the pediatric and adult individuals. Data were analyzed using one factor ANOVA and Fisher's post hoc least significant difference (PSLD) test to compare the choroidal thickness or volume in three or more groups. The correlations between choroidal thickness and systemic or ocular parameters were determined by Pearson's correlation tests for simple regression analysis and forward stepwise multiple regression analysis. The differences in the choroidal thickness between boys and girls were tested by $\chi^2$ tests. All analyses were done with the SPSS version 20.0 (SPSS Japan, Tokyo, Japan). A *P* value < 0.05 was considered statistically significant.

## RESULTS

None of the eyes was excluded because of unreliable measurements of the choroidal thickness. Even in pediatric individuals, none of the eyes was excluded because of eye movements during the scanning procedure.

### Comparisons of Choroidal Thickness and Volume Between Pediatric and Adult Individuals

The mean axial length in the pediatric individuals was significantly shorter than that in the adults ($P < 0.0001$, Table 1). The mean refractive error in the pediatric individuals was not significantly different from that of the adults ($P = 0.5256$).

The central choroidal thickness and volume within a 1.0-mm circle were significantly greater in the pediatric individuals (260.4 ± 57.2 μm, 0.205 ± 0.045 $mm^3$, respectively) than in the adults (206.1 ± 72.5 μm, 0.160 ± 0.056 $mm^3$, respectively; both $P < 0.0001$; Table 1). The macular choroidal thickness within a circle of 3.0- and 6.0-mm diameter in the children was significantly thicker than that of the adults (both $P < 0.0001$).

### Choroidal Thickness and Volume in ETDRS Sectors

In the pediatric individuals, the choroidal thicknesses in the four inner and four outer sectors were significantly different (both $P < 0.0001$, Table 2). The inner and outer nasal choroid

TABLE 2. Choroidal Thickness and Volume in ETDRS Grid Sectors in Pediatric and Adult Individuals

| | Pediatric Individuals | | Adult Individuals |
|---|---|---|---|
| Area | Choroidal Volume, $mm^3$ | Mean Choroidal Thickness, μm | Mean Choroidal Thickness, μm |
| Center | 0.205 ± 0.045 | 260.4 ± 57.2 | 206.1 ± 72.5 |
| Inner temporal | 0.423 ± 0.081* | 269.4 ± 51.9* | 206.3 ± 74.2 |
| Inner superior | 0.407 ± 0.086* | 259.1 ± 54.4* | 212.0 ± 70.6 |
| Inner inferior | 0.404 ± 0.084* | 257.1 ± 53.8* | 202.0 ± 74.7 |
| Inner nasal | 0.365 ± 0.091 | 232.2 ± 58.0 | 189.6 ± 70.5 |
| Outer temporal | 1.388 ± 0.238† | 262.0 ± 44.9† | 197.7 ± 69.2† |
| Outer superior | 1.327 ± 0.249† | 250.3 ± 47.0† | 213.4 ± 69.7† |
| Outer inferior | 1.300 ± 0.255† | 245.2 ± 48.1† | 194.6 ± 68.9† |
| Outer nasal | 0.971 ± 0.296 | 182.7 ± 53.0 | 147.8 ± 60.9 |

* Significantly larger than values of inner nasal area ($P < 0.005$).
† Significantly larger than values of outer nasal area ($P < 0.0001$).

Investigative Ophthalmology & Visual Science

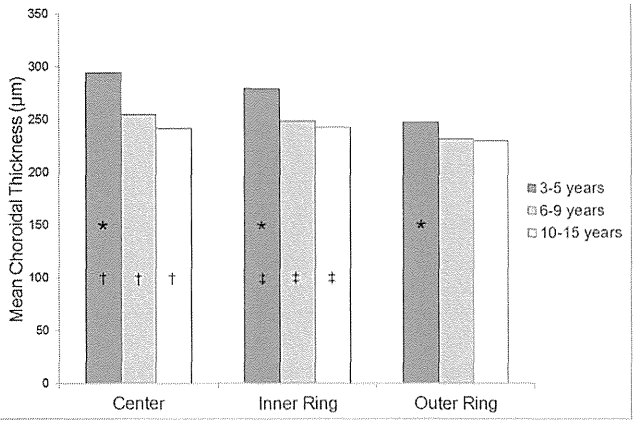


FIGURE 2. Pediatric choroidal thinning with increasing age in the central, inner ring, and outer ring areas of ETDRS grid. The mean choroidal thicknesses in the 3- to 5-year-old ($n = 25$), 6- to 9-year-old ($n = 42$), and 10- to 15-year-old ($n = 33$) age groups are presented. The choroidal thinning with increasing age appears to be more rapid in the central area than in the inner and outer rings. *$P = 0.0057$, †$P = 0.0011$, ‡$P = 0.0191$.

was significantly thinner than choroid of the other three inner and outer sectors (all $P < 0.005$). The choroidal thickness of the temporal sector was the thickest followed by the superior, inferior, and nasal choroid. However, differences among the temporal, superior, and inferior sectors of the inner and outer rings were not statistically significant.

In the adults, the choroidal thicknesses of the four inner sectors were not significantly different ($P = 0.2347$), but the outer choroidal thicknesses were significantly different among the four sectors ($P < 0.0001$). The outer nasal choroid was significantly thinner than that of the other three outer sectors (all $P < 0.0001$). The superior choroid was thickest, followed by the temporal, inferior, and nasal choroid; however, the majority of the differences were not significant.

Changes of the choroidal thickness maps associated with age are presented in Figure 2 and Table 3. In the pediatric individuals, the choroidal thinning with increasing age appeared to be more rapid in the central area than in the inner and outer rings (Fig. 2). The differences in the mean choroidal thicknesses among the 3- to 5-year-old, 6- to 9-year-old, and 10- to 15-year-old age groups were significant in the central and inner ring areas ($P = 0.0011$, $P = 0.0191$, respectively), but not in the outer ring area ($P = 0.2551$). The differences in the mean choroidal thicknesses of the central, inner ring, and outer ring areas were significant in the 3- to 5-year-old age group ($P = 0.0057$), but not in the 6- to 9-year-old and 10- to 15-year-old age groups ($P = 0.1081$, $P = 0.4401$, respectively), with a rapid decrease in the central

TABLE 3. Changes of the Mean Choroidal Thickness in ETDRS Grid Associated With Age

| | Eyes, *n* | Center, μm | Inner Ring, μm | Outer Ring, μm |
|---|---|---|---|---|
| Pediatric individuals | | | | |
| 3–15 y | 100 | 260.4 ± 57.2 | 254.4 ± 52.0 | 235.0 ± 43.3 |
| Adult individuals | | | | |
| 24–40 y | 25 | 247.7 ± 51.6 | 241.7 ± 49.8 | 229.1 ± 44.4 |
| 41–55 y | 14 | 221.5 ± 67.2 | 220.1 ± 63.4 | 203.4 ± 45.4 |
| 56–70 y | 19 | 190.1 ± 71.3 | 189.2 ± 68.1 | 172.8 ± 62.9 |
| 71–87 y | 25 | 168.1 ± 73.3 | 163.5 ± 69.4 | 151.1 ± 57.9 |

TABLE 4. Simple Regression Analysis for Correlations Between the Mean Choroidal Thickness of the Macular Area and the Age, Axial Length, Body Height, Body Weight, Body Mass Index, or Refractive Error in Pediatric Individuals

| | Central Choroidal Thickness, 1.0-mm Circle, μm | Macular Choroidal Thickness, 6.0-mm Circle, μm |
|---|---|---|
| Age, y | $r = -0.404$ | $r = -0.274$ |
| | $P < 0.0001$ | $P = 0.0056$ |
| Axial length, mm | $r = -0.525$ | $r = -0.448$ |
| | $P < 0.0001$ | $P < 0.0001$ |
| Body height, cm | $r = -0.419$ | $r = -0.299$ |
| | $P < 0.0001$ | $P = 0.0024$ |
| Body weight, kg | $r = -0.412$ | $r = -0.329$ |
| | $P < 0.0001$ | $P = 0.0008$ |
| Body mass index | $r = -0.293$ | $r = -0.272$ |
| | $P = 0.0030$ | $P = 0.0060$ |
| Refractive error, D | $r = 0.325$ | $r = 0.297$ |
| | $P = 0.0009$ | $P = 0.0025$ |

choroidal thickness. In pediatric and adult individuals. The most remarkable decrease in choroidal thickness was seen between the 41- to 55-year-old and 56- to 70-year-old groups, although some of the adult age groups had only a small number of eyes (Table 3).

## Simple Regression Analysis for Correlations Between Choroidal Thickness, and Systemic and Ocular Parameters in Pediatric Individuals

Simple linear regression analysis showed that the central choroidal thickness was correlated significantly with the age, axial length, body height, body weight, body mass index, and refractive error (all $P < 0.005$, Table 4). The central choroidal thickness was significantly thicker in girls (274.1 ± 62.1 μm) than in boys (247.9 ± 46.6 μm, $P = 0.0255$). The correlations between the macular choroidal thickness within a circle of 6.0-mm diameter and systemic and ocular parameters were similar to the results for the central choroidal thickness (Table 4).

## Multiple Regression Analysis for Correlations Between Choroidal Thickness, and Systemic and Ocular Parameters in Pediatric Individuals

Multiple linear regression analysis of the mean central choroidal thickness by age, axial length, body height, body weight, body mass index, and refractive error was performed. A forward stepwise method was used to determine factors associated most with the choroidal thickness. The highest correlation was between the choroidal thickness, and the axial length and body mass index, with a determination coefficient ($R^2$) of 0.313 ($P < 0.0001$, Fig. 3). Using analysis of covariance, the effects of the age group (pediatric or adult group), axial length, and body mass index on the central choroidal thickness were evaluated. After adjustment for the axial length and body mass index, the central choroidal thickness was no longer significantly correlated with the age group ($P = 0.632$).

## Interobserver Reproducibility of Choroidal Thickness

In all the pediatric and adult individuals, manual segmentation was performed in 180 of the 183 eyes. Proportion of the scans needed for manual segmentation to all the 64 scans was calculated in each subject. The mean percentage of manual

Investigative Ophthalmology & Visual Science

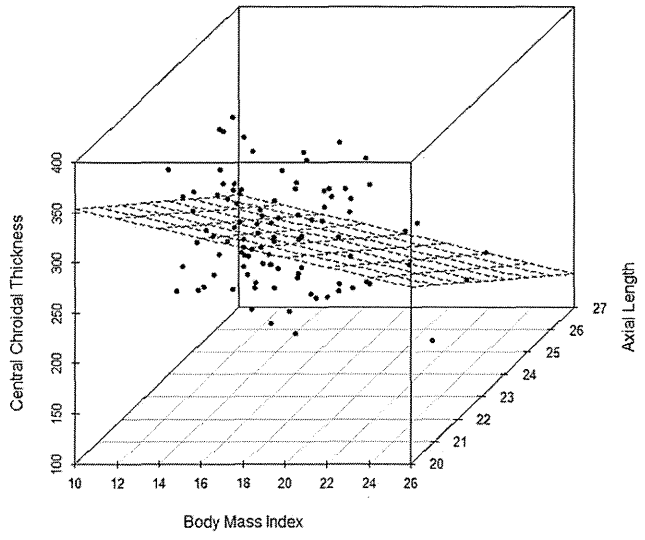


FIGURE 3. Three-dimensional scatterplot of the body mass index ($x$-axis), central choroidal thickness ($y$-axis), and axial length ($z$-axis). The model shows a relatively good coefficient of determination ($R^2 = 0.313$, $P < 0.0001$). Mean central choroidal thickness = 807.933 − 20.229 × axial length − 4.906 × body mass index.

segmentation required was 25.1 ± 20.7%. A proper tracing of the RPE was confirmed in all images of all subjects.

Before this study, the chorioscleral border was corrected independently by the two observers in 14 pediatric individuals.[15] The ICCs for the mean choroidal thickness of each ETDRS grid sector that was measured by the two observers are shown in Table 5. The mean choroidal thickness had a high ICC (from 0.9908–0.9995) between the two observers ($P <$ 0.0001).

For the Bland and Altman plots, the mean difference in the choroidal thickness of the nine ETDRS grid sectors between Observer 1 and Observer 2 varied from −1.9 to 2.9 μm. The 95% LoA for all the ETDRS sectors including zero showed that no fixed bias was present (Table 5). In all of the ETDRS sectors, the mean of choroidal thickness calculated by Observer 1 and Observer 2 was not correlated significantly with the mean difference between the two measurements (Observer 1 − Observer 2, all $P > 0.05$). Thus, no proportional bias was considered to be present.

## DISCUSSION

Our findings showed that high ICC values were found between the two observers, and the results of Bland-Altman plots indicated the highly reproducible measurements of the choroidal thickness with semiautomatic segmentation. These findings indicated that we can obtain valid and reproducible results of the choroidal thickness of the images obtained by SS-OCT.

Park and Oh[20] reported that the pediatric subfoveal choroidal thickness determined by EDI-OCT was 343.1 ± 79.8 μm. However, the choroidal thickness was measured in a point-by-point way and did not include comparisons with adult subjects. Ruiz-Moreno et al.[19] examined the choroidal thickness in 43 normal pediatric patients using a prototype SS-OCT instrument. They reported that the mean macular choroidal thickness in the pediatric patients (285.2 ± 56.7 μm) was not significantly thicker than that in healthy adults (275.2 ± 92.7 μm, $P = 0.08$). However, they measured the choroidal thickness at only 7 points in the horizontal plane. In addition,

TABLE 5. ICCs and Results of Bland-Altman Method in Choroidal Thickness of ETDRS Grid Sectors Measured by Two Observers in 14 Selected Pediatric Individuals

| Area | ICC ($P$ Value) | 95% LoA | Correlation Between Mean and Mean Difference |
|---|---|---|---|
| Center | 0.9979 (<0.0001) | −13.5~11.5 | $r = -0.260$, $P = 0.3783$ |
| Inner temporal | 0.9995 (<0.0001) | −5.4~4.8 | $r = -0.271$, $P = 0.3563$ |
| Inner superior | 0.9908 (<0.0001) | −20.8~17.1 | $r = -0.207$, $P = 0.4869$ |
| Inner inferior | 0.9992 (<0.0001) | −7.2~6.9 | $r = -0.147$, $P = 0.6224$ |
| Inner nasal | 0.9962 (<0.0001) | −16.1~12.9 | $r = -0.308$, $P = 0.2908$ |
| Outer temporal | 0.9945 (<0.0001) | −9.6~14.6 | $r = -0.234$, $P = 0.4284$ |
| Outer superior | 0.9931 (<0.0001) | −12.6~18.4 | $r = 0.356$, $P = 0.2169$ |
| Outer inferior | 0.9993 (<0.0001) | −7.0~5.6 | $r = -0.513$, $P = 0.0602$ |
| Outer nasal | 0.9953 (<0.0001) | −13.9~17.2 | $r = 0.151$, $P = 0.6129$ |

The 95% LoA, expected difference between two measurements was calculated as the mean of the differences ± 1.96 × SD of the differences.

the mean age of their pediatric subjects was 10 ± 3 years, which is older than that of our group. Moreover, both eyes were included in their analyses, which can lead to bias. We examined the mean choroidal thickness and volume in one randomly selected eye of all subjects to create the choroidal thickness maps.

Using EDI-OCT, Read et al.[21] recently reported that the choroidal thickness increased significantly from early childhood to adolescence. However, only children with refractive error between +1.25 and −0.50 D were studied, thereby minimizing the potential influence of refractive error or axial length on the choroidal thickness. Indeed, the investigators reported that a strong negative association between axial length and choroidal thickness would be expected to result in a decrease in choroidal thickness with increasing age, rather than an increase in choroidal thickness. They concluded that longitudinal studies of the choroidal thickness in childhood, including myopic participants, will be necessary.

An earlier study reported that the axial length increased by 3 mm between the ages of 9 months and 9 years.[30] Because the choroidal thickness decreases with increases in the axial length in healthy adults,[11,15,16] the choroidal thickness in children is assumed to be thicker than that of adults. We found that the macular choroid was significantly thicker and the volume significantly larger in the pediatric individuals than in the adults. After adjustment for axial length and body mass index, the central choroidal thickness was no longer significantly correlated with the age group. This suggests that the pediatric choroidal thickening may be influenced by the shortening of the axial length and low body mass index. Hirata et al.[15] reported that the central choroidal thickness was 202.6 ± 83.5 μm in adults, which is comparable to the 206.1 ± 72.5 in our study.

The sectorial choroidal thicknesses were slightly different in the pediatric and adult individuals. Although the thinnest area was nasal in both groups, the thickest area was temporal in the

Investigative Ophthalmology & Visual Science

children and superior in the adults. Ruiz-Moreno et al.[19] reported that the pediatric choroidal thickness along the horizontal line was thicker on the temporal side than in the fovea, and it was thinnest on the nasal side. In addition, the adult choroidal thickness in their study was thickest in the fovea, followed by the temporal, and it was thinnest on the nasal side. These results are consistent with our results.

The thinning of pediatric choroid with increasing age appeared to occur more quickly in the central area. Moreno et al.[31] reported that the central choroidal thickness in newborn infants (329 ± 66 μm) was remarkably thicker than that in adults (258 ± 66 μm). In their study, the subfoveal choroid in the newborn infant was significantly thicker than the superior or inferior choroid at 2000 μm from the fovea, and the mean difference between subfoveal and superior choroidal thickness was 87 μm. These results are consistent with our findings.

To the best of our knowledge, there has been only one report on the choroidal volume measured by SS-OCT in adults.[15] The choroidal volume can reflect the vascular changes, for example, vascular hyperpermeability or vasodilation, that can be observed in retinochoroidal diseases, such as central serous chorioretinopathy.[4] At present, the status of the choroid usually is evaluated by the choroidal thickness measured at a few points. However, point-by-point measurements can be affected by focal thickening or thinning of the choroid,[22,23] or by irregularities of the chorioscleral border.[5] Examining the choroidal volume by 3D mapping is a better method for a comprehensive evaluation of the entire macular area.

In pediatric individuals, Ruiz-Moreno et al.[19] reported that the average choroidal thickness at 7 horizontal points of the macular area was correlated significantly with the age and refractive error. We found that the mean central choroidal thickness was correlated significantly with the age, axial length, body height, body weight, body mass index, and refractive error using simple linear regression analyses. In addition, multiple linear regression analysis with the forward stepwise method showed that the model determined by the axial length and body mass index had the highest regression coefficients. In schoolchildren, Selovic et al.[32] found that the axial length increased with increasing age, body height, and weight, but was more highly correlated with the height and weight than with the age. This close relationship between axial length and body height or weight may contribute to the relationship between pediatric choroidal thickness and body mass index, because the axial length is known to be correlated closely with the choroidal thickness.[11,15,16]

A choroidal thickness map of the macular area was created by semiautomatic segmentation. Manual segmentation was performed in 25.1 ± 20.7% of our eyes because of errors in the delineation of the chorioscleral border by the built-in software. To standardize this evaluation further, it will be necessary that a choroidal thickness map can be created by fully automatic segmentation. For this purpose, a software to determine chorioscleral border more accurately and further improvement of the OCT image quality are essential.

One of the limitations of our study was that we examined only Japanese subjects, and the choroidal thickness in children of other races was not determined. In addition, the relatively small sample size might be insufficient to evaluate choroidal thicknesses in a pediatric population.

In conclusion, the macular choroid was significantly thicker and the volume was significantly larger in pediatric individuals than in adults. Although the thinnest area was nasal in both groups, the thickest area was temporal in the children and superior in the adults. Pediatric choroidal thinning with increasing age appears to be more rapid in the central sector than in the outer sectors. Pediatric choroidal thickness was associated significantly with systemic and ocular parameters, especially the axial length and body mass index. Further studies in a larger number of pediatric individuals will be needed to determine precisely the choroidal status in pediatric eyes.

## Acknowledgments

The authors alone are responsible for the content and writing of the paper.

Disclosure: **T. Nagasawa**, None; **Y. Mitamura**, None; **T. Katome**, None; **K. Shinomiya**, None; T. **Naito**, None; **D. Nagasato**, None; **Y. Shimizu**, None; **H. Tabuchi**, None; **Y. Kiuchi**, None

## References

1. Spaide RF, Koizumi H, Pozzoni MC. Enhanced depth imaging spectral-domain optical coherence tomography. *Am J Ophthalmol*. 2008;146:496–500.
2. Spaide RF. Enhanced depth imaging optical coherence tomography of retinal pigment epithelial detachment in age-related macular degeneration. *Am J Ophthalmol*. 2009;147:644–652.
3. Margolis R, Spaide RF. A pilot study of enhanced depth imaging optical coherence tomography of the choroid in normal eyes. *Am J Ophthalmol*. 2009;147:811–815.
4. Imamura Y, Fujiwara T, Margolis R, Spaide RF. Enhanced depth imaging optical coherence tomography of the choroid in central serous chorioretinopathy. *Retina*. 2009;29:1469–1473.
5. Chung SE, Kang SW, Lee JH, Kim YT. Choroidal thickness in polypoidal choroidal vasculopathy and exudative age-related macular degeneration. *Ophthalmology*. 2011;118:840–845.
6. Fong AH, Li KK, Wong D. Choroidal evaluation using enhanced depth imaging spectral-domain optical coherence tomography in Vogt-Koyanagi-Harada disease. *Retina*. 2011;31:502–509.
7. Ohno-Matsui K, Akiba M, Moriyama M, Ishibashi T, Tokoro T, Spaide RF. Imaging retrobulbar subarachnoid space around optic nerve by swept-source optical coherence tomography in eyes with pathologic myopia. *Invest Ophthalmol Vis Sci*. 2011;52:9644–9650.
8. Spaide RF, Akiba M, Ohno-Matsui K. Evaluation of peripapillary intrachoroidal cavitation with swept source and enhanced depth imaging optical coherence tomography. *Retina*. 2012;32:1037–1044.
9. Wojtkowski M, Srinivasan V, Ko T, Fujimoto J, Kowalczyk A, Duker J. Ultrahigh-resolution, high-speed, Fourier domain optical coherence tomography and methods for dispersion compensation. *Opt Express*. 2004;12:2404–2422.
10. Nagasawa T, Mitamura Y, Katome T, Nagasato D, Tabuchi H. Swept-source optical coherence tomographic findings in morning glory syndrome [published online ahead of print May 28, 2013]. *Retina*.
11. Ikuno Y, Kawaguchi K, Nouchi T, Yasuno Y. Choroidal thickness in healthy Japanese subjects. *Invest Ophthalmol Vis Sci*. 2010;51:2173–2176.
12. Potsaid B, Baumann B, Huang D, et al. Ultrahigh speed 1050 nm swept source/Fourier domain OCT retinal and anterior segment imaging at 100,000 to 400,000 axial scans per second. *Opt Express*. 2010;18:20029–20048.
13. Srinivasan VJ, Huber R, Gorczynska I, et al. High-speed, high resolution optical coherence tomography retinal imaging with a frequency-swept laser at 850 nm. *Opt Lett*. 2007;32:361–363.
14. Yasuno Y, Hong Y, Makita S, et al. In vivo high-contrast imaging of deep posterior eye by 1-micron swept source optical coherence tomography and scattering optical coherence angiography. *Opt Express*. 2007;15:6121–6139.

15. Hirata M, Tsujikawa A, Matsumoto A, et al. Macular choroidal thickness and volume in normal subjects measured by swept-source optical coherence tomography. *Invest Ophthalmol Vis Sci.* 2011;52:4971–4978.
16. Ding X, Li J, Zeng J, et al. Choroidal thickness in healthy Chinese subjects. *Invest Ophthalmol Vis Sci.* 2011;52:9555–9560.
17. Ouyang Y, Heussen FM, Mokwa N, et al. Spatial distribution of posterior pole choroidal thickness by spectral domain optical coherence tomography. *Invest Ophthalmol Vis Sci.* 2011;52:7019–7026.
18. Manjunath V, Taha M, Fujimoto JG, Duker JS. Choroidal thickness in normal eyes measured using Cirrus HD optical coherence tomography. *Am J Ophthalmol.* 2010;150:325–329.
19. Ruiz-Moreno JM, Flores-Moreno I, Lugo F, Ruiz-Medrano J, Montero JA, Akiba M. Macular choroidal thickness in normal pediatric individuals measured by swept-source optical coherence tomography. *Invest Ophthalmol Vis Sci.* 2013;54:353–359.
20. Park KA, Oh SY. Analysis of spectral-domain optical coherence tomography in preterm children: retinal layer thickness and choroidal thickness profiles. *Invest Ophthalmol Vis Sci.* 2012;53:7201–7207.
21. Read SA, Collins MJ, Vincent SJ, Alonso-Caneiro D. Choroidal thickness in childhood. *Invest Ophthalmol Vis Sci.* 2013;54:3586–3593.
22. Yeoh J, Rahman W, Chen F, et al. Choroidal imaging in inherited retinal disease using the technique of enhanced depth imaging optical coherence tomography. *Graefes Arch Clin Exp Ophthalmol.* 2010;248:1719–1728.
23. Yasuno Y, Okamoto F, Kawana K, Yatagai T, Oshika T. Investigation of multifocal choroiditis with panuveitis by three-dimensional high-penetration optical coherence tomography. *J Biophotonics.* 2009;2:435–441.
24. Early Treatment Diabetic Retinopathy Study research group. Photocoagulation for diabetic macular edema. Early Treatment Diabetic Retinopathy Study report number 1. *Arch Ophthalmol.* 1985;103:1796–1806.
25. Brown JS, Flitcroft DI, Ying GS, et al. In vivo human choroidal thickness measurements: evidence for diurnal fluctuations. *Invest Ophthalmol Vis Sci.* 2009;50:5–12.
26. Tan CS, Ouyang Y, Ruiz H, Sadda SR. Diurnal variation of choroidal thickness in normal, healthy subjects measured by spectral domain optical coherence tomography. *Invest Ophthalmol Vis Sci.* 2012;53:261–266.
27. Agawa T, Miura M, Ikuno Y, et al. Choroidal thickness measurement in healthy Japanese subjects by three-dimensional high-penetration optical coherence tomography. *Graefes Arch Clin Exp Ophthalmol.* 2011;249:1485–1492.
28. Bland JM, Altman DG. Statistical methods for assessing agreement between two methods of clinical measurement. *Lancet.* 1986;1:307–310.
29. Katome T, Mitamura Y, Nagasawa T, Eguchi H, Naito T. Quantitative analysis of cystoid macular edema using scanning laser ophthalmoscope in modified dark-field imaging. *Retina.* 2012;32:1892–1899.
30. Twelker JD, Mitchell GL, Messer DH, et al. Children's ocular components and age, gender, and ethnicity. *Optom Vis Sci.* 2009;86:918–935.
31. Moreno TA, O'Connell RV, Chiu SJ, et al. Choroid development and feasibility of choroidal imaging in the preterm and term infants utilizing SD-OCT. *Invest Ophthalmol Vis Sci.* 2013;54:4140–4147.
32. Selovic A, Juresa V, Ivankovic D, Malcic D, Selovic Bobonj G. Relationship between axial length of the emmetropic eye and the age, body height, and body weight of schoolchildren. *Am J Hum Biol.* 2005;17:173–177.

Investigative Ophthalmology & Visual Science

OPEN ACCESS Freely available online

PLOS | ONE

# The Whole Macular Choroidal Thickness in Subjects with Primary Open Angle Glaucoma

**Shunsuke Nakakura[1]*, Minami Yamamoto[1], Etsuko Terao[1], Toshihiko Nagasawa[1], Hitoshi Tabuchi[1], Yoshiaki Kiuchi[2]**

**1** Department of Ophthalmology, Saneikai Tsukazaki Hospital, Himeji, Japan, **2** Department of Ophthalmology and Visual Sciences, Graduate School of Biomedical Sciences, Hiroshima University, Hiroshima, Japan

## Abstract

*Purpose:* We investigated the whole macular choroidal thickness in subjects with glaucoma in order to evaluate the effects of glaucoma and glaucoma visual field damage on the choroidal thickness.

*Subjects and Methods:* We examined 40 primary open angle glaucoma patients with only superior visual field defects and 48 normal controls. The macular choroidal thickness was measured using swept-source optical coherence tomography according to the three-dimensional raster scan protocol (6×6 mm). We used the choroidal thickness within a 1.0-mm circle measured on ETDRS grids as the central sector and then used a 6×6 rectangular grid to divide the area into six sectors.

*Results:* No significant differences were found in the choroidal thickness values between the glaucoma and normal subjects in any of the sectors after adjusting for the age and axial length (all $P>0.4$, ANCOVA). According to a stepwise analysis of the glaucoma subjects performed using the parameters of age, axial length, central corneal thickness and mean deviation (MD value) obtained by static perimetry, age was the most predictive and significant factor in all sectors (coefficient = −3.091 to −4.091 and F value = 15.629 to 22.245), followed by axial length (coefficient = −10.428 to −23.458 and F value = 2.454 to 6.369). The central corneal thickness and MD values were not significant predictive factors in any of the sectors. No significant predictive factors were found for the differences in the choroidal thickness values observed between the superior and inferior field sectors.

*Conclusions:* Neither the glaucoma-related visual field damage nor glaucoma itself have any apparent associations with the whole macular choroidal thickness.

*Trial Registration:* Japan Clinical Trials Register (http://www.umin.ac.jp/ctr/ number, UMIN 000012527).

**Citation:** Nakakura S, Yamamoto M, Terao E, Nagasawa T, Tabuchi H, et al. (2014) The Whole Macular Choroidal Thickness in Subjects with Primary Open Angle Glaucoma. PLoS ONE 9(10): e110265. doi:10.1371/journal.pone.0110265

**Editor:** Demetrios Vavvas, Massachusetts Eye & Ear Infirmary, Harvard Medical School, United States of America

**Received** July 16, 2014; **Accepted** September 10, 2014; **Published** October 28, 2014

**Copyright:** © 2014 Nakakura et al. This is an open-access article distributed under the terms of the Creative Commons Attribution License, which permits unrestricted use, distribution, and reproduction in any medium, provided the original author and source are credited.

**Data Availability:** The authors confirm that all data underlying the findings are fully available without restriction. All relevant data are within the paper and its Supporting Information files.

**Funding:** The authors have no support or funding to report.

**Competing Interests:** The authors have declared that no competing interests exist.

* Email: shunsukenakakura@yahoo.co.jp

## Introduction

Whether the choroidal thickness is truly associated with the etiology or progression of glaucoma remains unknown. The uvea (choroid, iris and ciliary body) contains abundant large and small vessels, and utilizes more than 80% of the ocular blood flow [1]. The factors that influence the ocular blood flow, such as a low systolic perfusion pressure, low systolic blood pressure and history of cardiovascular disease, have been reported to be predictors of long-term glaucoma progression [2]. Recently, the development of enhanced-depth imaging optical coherence tomography (OCT) based on spectral-domain OCT has enabled clinicians to measure the choroidal thickness noninvasively. Previous studies have reported that a thinner choroidal thickness value at the fovea is associated with an older age [3–9], longer axial length [3–6,8,9] and thicker central corneal thickness (CCT) [6,9].

With respect to the association between glaucoma and the choroidal thickness, previous reports have shown no significant differences between glaucoma patients and normal subjects [5,7,9] or among individuals suspected of having glaucoma [6] based on the choroidal thickness value. However, Hirooka et al. reported that, in the setting of normal tension glaucoma (NTG), which was diagnosed when there was an untreated peak IOP≤21 mmHg, including the 24-h fluctuations, there was choroidal thinning 3 mm nasal from the fovea compared with that observed in normal subjects [10]. Meanwhile, Usui et al. reported that, in highly myopic eyes (with a spherical equivalent refractive error between -6 and -12 diopters, and an axial length greater than 26.5 mm), NTG patients exhibit thinner choroidal values at the fovea and around the optic disc than subjects without glaucoma [11]. However, even if the choroidal thinning or thickening is associated with glaucoma, whether such changes in the choroidal

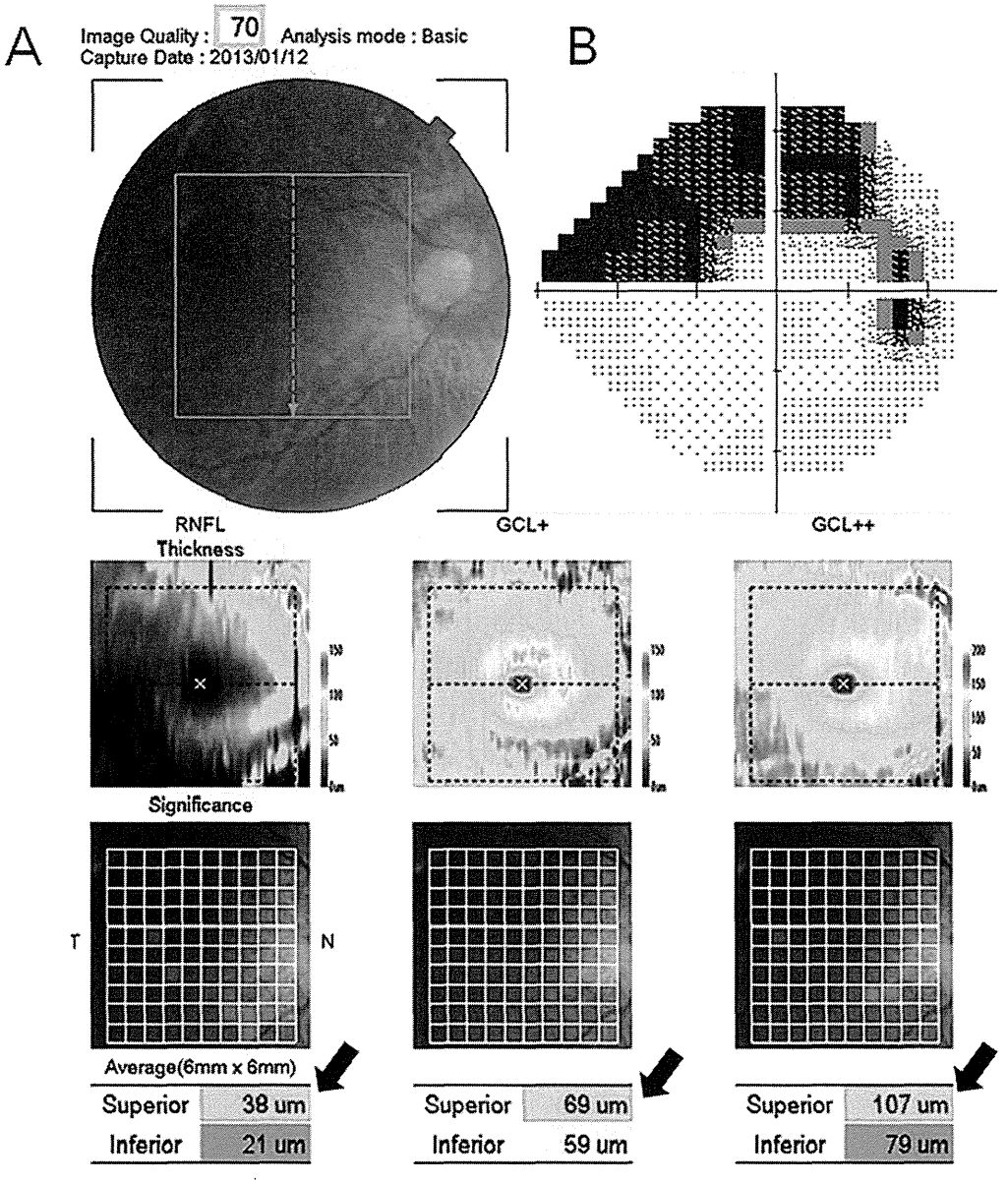


**Figure 1. The 3D-OCT map and results of the HFA test in a 71-year-old male subject with glaucoma.** (A) The 3D-OCT map provides a 10×10 grid map of the macular RNFL (GCL+), ganglion cell layer (GCL)/inner plexiform layer (IPL) thickness (GCL++) and macular RNFL+GCL+IPL. Upper panel: a pseudo-colored map of the measured thickness. Center panel: Each grid in the 10×10 grid was color-coded, with no color (within the normal limit), yellow (outside of the 95% normal limit) or red (outside of the 99% normal limit) used to indicate different values. Lower panel: the thicknesses of the total, superior and inferior hemiretinal sectors. The black arrows show the superior hemiretinal thickness, which is displayed as color-coded with green (within the normal limit), yellow (outside of the 95% normal limit) or red (outside of the 99% normal limit) based on the software program's normal built-in dataset. (B) The results of the HFA test. The MD was −9.38 dB ($P<0.5\%$) and the PSD was 14.54 dB ($P<0.5\%$). Superior glaucoma visual field damage corresponds to inferior optic disc rim thinning and the 3D-OCT data. The inferior visual field was intact.
doi:10.1371/journal.pone.0110265.g001

thickness values are primary or occur secondarily due to the progression of glaucoma remains unknown.

Furthermore, most of the previous reports have focused on the subfoveal choroidal thickness and/or choroidal thickness values at +/− 3 mm nasal or temporal to the fovea. Glaucoma is generally characterized by optic disc changes with corresponding nerve fiver defects and visual field defects. The initial changes most frequently occur in the inferior optic disc rim, corresponding to a superior visual field defect, and it does not exceed the central line, since the normal retinal nerve fiber layers run symmetrically in the superior and inferior fields. However, the fovea is free of a nerve fiber layer, as the inner retina and ganglion cells are pushed away to the foveal slope. Therefore, the use of measurement points at the fovea or +/− 3 mm nasal or temporal to the fovea may not be appropriate for evaluating the relationship between glaucoma and the choroidal thickness.

Swept-source optical coherence tomography (SS-OCT) applies a swept wavelength laser as a light source [12,13], with a longer center wavelength that penetrates deeply into tissues. The longer wavelength (1,050 mm) of SS-OCT is attenuated by water absorption; however, SS-OCT can achieve much less roll-off, thus leading to retained sensitivity at increasing depths, and can

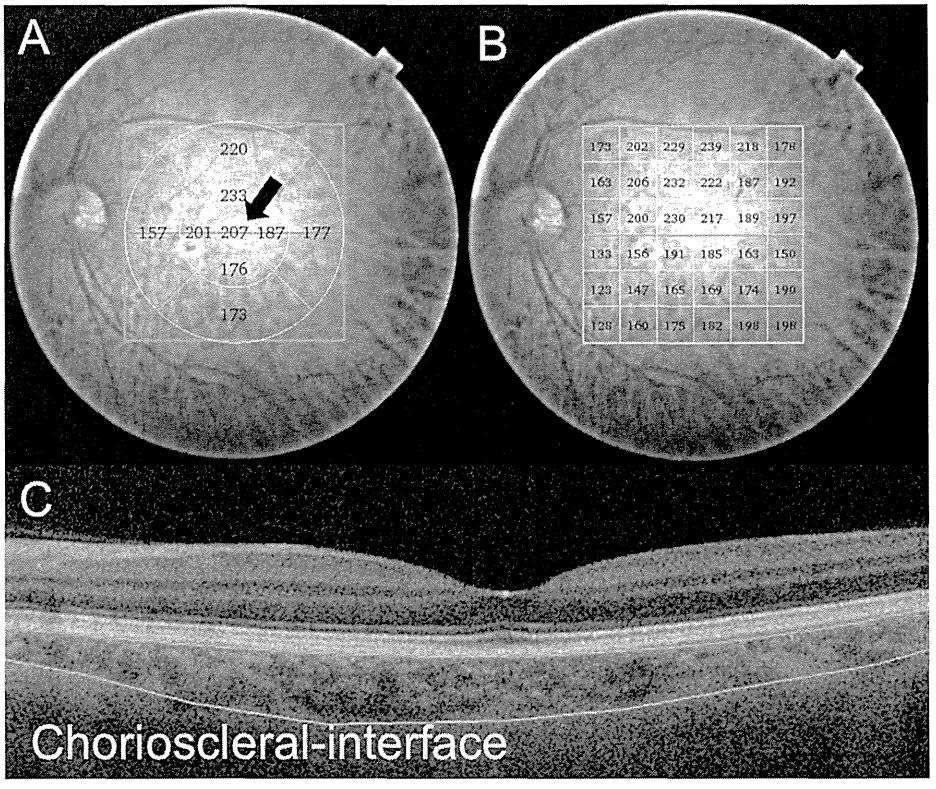


**Figure 2. The choroidal thickness map of a 57-year-old normal male obtained using SS-OCT.** The 3D raster scan protocol with 512A-scans ×256 B-scans was used to obtain the 3D imaging data for a 6×6-mm area. (A) The black arrow shows the central sector choroidal thickness as measured on the ETDRS grid within a 1×1-mm circular area. (B) The choroidal thickness values presented by the 6×6 rectangular grid map. Each value shows the mean choroidal thickness within a 1×1-mm square area. (C) Manual segmentation of the chorioscleral interface on the B-scan image. All 64 B-scan images were obtained for each subject.
doi:10.1371/journal.pone.0110265.g002

operate at a higher speed than spectral domain OCT to obtain the choroidal thickness maps using the 3D raster scan protocol [14].

The aim of this study was to investigate the whole macular choroidal thickness (6×6 mm) in patients with superior glaucoma visual hemi-field defects in order to: 1) compare these values with those observed in normal subjects after adjusting for the previously identified factors associated with the choroidal thickness (age and axial length) and 2) to investigate whether the degree of glaucoma visual field damage is associated with the choroidal thickness and/

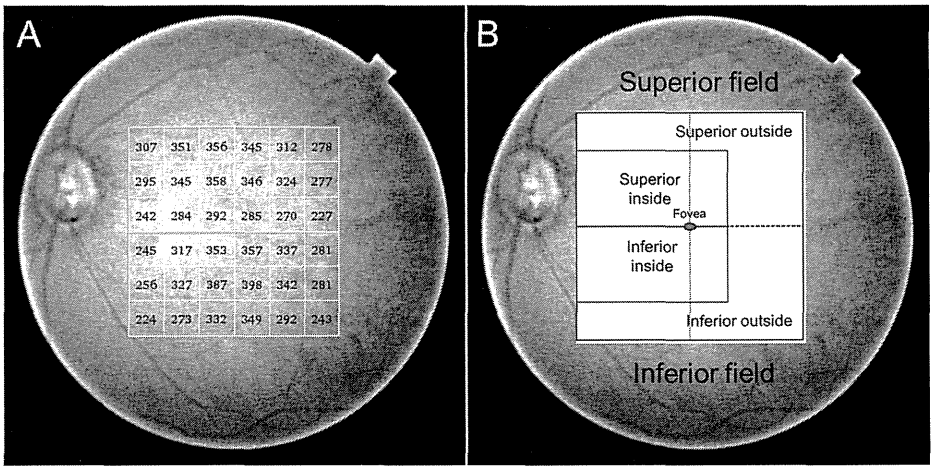


**Figure 3. The choroidal thickness map of a 74-year-old female subject with glaucoma obtained using SS-OCT.** (A) The choroidal thickness values presented on the 6×6 rectangular grid map. (B) The six sectors used in the present study. Each area was symmetrically divided between the superior and inferior sectors by a horizontal line.
doi:10.1371/journal.pone.0110265.g003

or differences in the choroidal thickness values between the superior and inferior sectors.

## Subjects and Methods

We studied 88 subjects (40 glaucoma patients and 48 normal subjects) treated at Saneikai Tsukazaki Hospital from October 2012 to December 2013. This study received approval from the Institutional Review Board of Saneikai Tsukazaki Hospital and was performed according to the tenets of the Declaration of Helsinki. Written informed consent was obtained from each participant prior to enrollment in this study. All subjects received a full ophthalmic examination (conducted by S.N. or T.N) and had a best-correlated visual acuity of more than 0.6, refractive errors (spherical equivalent) within ±6 diopters (D) and cylinder correction within ±3D. The refraction was measured using an autorefractor (KR-8800, Topcon Corporation, Japan). The axial length (AL) was measured using an IOLMaster, ver. 5.02 (Carl Zeiss Meditec, Jena, Germany), and the mean of five measurements was used in the subsequent analyses. The CCT values in the glaucoma subjects were measured with a specular microscope (SP-3000, Topcon Corporation, Japan). The intraocular pressure was measured using a Goldmann applanation tonometer with the subject in the sitting position.

All glaucoma patients had attended our clinic for at least one year and their disease was well controlled with topical anti-glaucoma eye drops. Each patient received a reliable visual field analysis (Humphry Visual Field Analyzer (HFA), Carl Zeiss Inc., Dublin, CA) according to the thresholding algorithm (SITA-standard) 30-2, and underwent HFA at four- to six-month intervals. The visual field test results used in the study were obtained within ± three months of the time when the choroidal thickness was measured, and which had fixation losses less than 20%, and the false-positive and false-negative errors were less than 15%. A glaucomatous visual field defect was defined as 1) a glaucoma hemifield test graded "outside the normal limits" and 2) a cluster of three contiguous points at the 5% level for the pattern deviation plot, with at least one point being $P<1\%$. The mean deviation value (MD value) was used for the analysis. All patients had primary open angle glaucoma, as defined by 1) the results of a gonioscopic examination that revealed an open angle and 2) the presence of visual field defects in least one of the eyes whose locations corresponded to glaucomatous disc excavation, namely, the presence of a focal or diffuse defect of the optic disc rim with or without retinal nerve fiver layer (RNFL) defects.

In the present study, we recruited glaucoma patients who exhibited only focal or diffuse inferior optic rim thinning with corresponding superior visual field loss. Patients with a history of any previous glaucoma surgery or systemic diseases, such as diabetes mellitus or uncontrolled hypertension, the use of an oral carbonic anhydrase inhibitor (acetazolamide) and/or an unknown previous refraction before cataract surgery were excluded. Patients who displayed any optic disc changes suspected to be due to glaucoma at the superior optic disc rim confirmed based on the presence of ganglion cell-loss on three-dimensional OCT were also excluded (3D-OCT; Topcon, Inc., Tokyo, Japan). The 3D-OCT provides a 10×10 grid map of the macula RNFL and ganglion cell layer (GCL)/inner plexiform layer (IPL) thickness, and uses a software program that displays a deviation map indicating if there is a significant reduction of the total macular retinal thickness, superior hemiretinal thickness or inferior hemiretinal thickness compared to that observed in a built-in normal database in three areas (the mean macular RNFL, mean GCL/IPL and mean macular RNFL+ mean GCL/IPL), with a probability of less than 1% [15]. All glaucoma patients exhibited only inferior hemiretinal thickness abnormalities (displayed in yellow or red), with a normal superior hemiretinal thickness (displayed in green). Figure 1 shows the macular retinal thickness values in the glaucoma patients measured on 3D-OCT and the glaucoma visual field defects measured on HFA (The 3D-OCT data are provided in Table S1).

The inclusion criteria for normal subjects were 1) IOP ≤21 mm Hg 2) normal ophthalmoscopic appearance of the optic nerve (cup-to-disc ratio <0.5 in both eyes, cup-to disc ratio asymmetry <0.2, the absence of hemorrhage, or the presence of localized or diffuse rim thinning).[5] The exclusion criteria for the normal controls were as follows: 1) a history of intraocular surgery, 2) a history or evidence of chorioretinal or vitreoretinal disease and 3) systemic disease, such as diabetes mellitus or uncontrolled hypertension. Normal subjects did not undergo HFA testing.

### Swept-source Optical Coherence Tomography (SS-OCT)

The macula area (6×6mm) of the eyes was examined with the SS-OCT instrument (DR1 OCT-1; Topcon, Tokyo, Japan). The SS-OCT has an acquisition rate of 100,000 A-scans per second when operated with the 1-μm wavelength tunable laser centered at 1,050 nm, with an approximate 100-nm tuning range and a tissue imaging depth of 2.6 mm [14]. Following pupil dilation, the SS-OCT examinations were performed by experienced certified orthoptists (M.Y and E.T) from 1:00 PM to 5:00 PM to reduce the effects of diurnal fluctuations [16,17]. The 3D volumetric raster

**Table 1.** The patient demographics.

| | Glaucoma N = 40 | | Normal N = 48 | | |
|---|---|---|---|---|---|
| | mean ±SD | range | mean ±SD | range | P value |
| Age (years) | 65.2±11.8 | 40–85 | 66.4±11.8 | 31–87 | 0.631* |
| Sex/female (%) | 31(78) | | 24(50) | | 0.007† |
| Right eye (%) | 19(47) | | 27(56) | | 0.413† |
| IOP (mmHg) | 15.8±2.6 | 12–21 | 15.6±2.8 | 9–21 | 0.832* |
| Axial length (mm) | 23.7±1.2 | 20.6–26.0 | 23.9±1.1 | 21.8–27.6 | 0.514* |
| CCT (μm) | 502.9±28.9 | 445–558 | - | - | - |
| Mean deviation (dB) | −5.1±4.7 | −19.64–0.24 | - | - | - |

*, Student's *t*-test
†, chi-square test.
doi:10.1371/journal.pone.0110265.t001

**Table 2.** Comparisons among the sectors between the glaucoma and normal groups.

| | Glaucoma | 95% CI | Normal | 95% CI | P value |
|---|---|---|---|---|---|
| The central sector | 219.1±11.2 | 196.7–241.6 | 216.6±10.2 | 196.1–237.1 | 0.869 |
| a: superior field ave | 208.6±8.9 | 190.8–226.5 | 200.9±8.1 | 184.6–217.2 | 0.531 |
| b: inferior field ave | 193.2±9.1 | 174.9–211.5 | 185.4±8.3 | 168.8–202.1 | 0.536 |
| c: superior inside ave | 198.8±9.9 | 179.1–218.5 | 193.8±9.0 | 175.8–211.8 | 0.712 |
| d: superior outside ave | 216.7±8.5 | 199.7–233.6 | 206.6±7.7 | 191.1–222.1 | 0.390 |
| e: inferior inside ave | 188.0±10.1 | 167.8–208.1 | 183.0±9.2 | 164.7–201.4 | 0.720 |
| f: inferior outside ave | 197.3±8.7 | 179.8–214.7 | 187.4±8.0 | 171.4–203.3 | 0.408 |

Ave, average.
The data are presented as the age- and axial length-adjusted mean ± standard error of the mean (SEM) and 95% CI (confidence interval) (μm).
All P values were obtained with an ANCOVA using the age and axial length as covariates.
doi:10.1371/journal.pone.0110265.t002

scan protocol was used, which covered an area measuring 6×6 mm centered on the fovea, with 512 A-scans × 256 B-scans. All images had image quality scores ≥45 (of 160), according to the manufacturer's recommendations.

Using a series of 64 B-scan images, each of which was created by averaging four consecutive B-scans, a choroidal thickness map was created via semiautomatic segmentation. The choroidal thickness was measured as the distance from the outer border of the retinal pigment epithelium to the inner surface of the chorioscleral interface. However, semiautomatic segmentation does not always provide the correct chorioscleral interface; therefore, manual segmentation using the built-in software program was performed on all 64 B-scan images in each patient by experienced certified orthoptists (M.Y and E.T). The interobserver reproducibility of the choroidal thickness values obtained using this manual segmentation method has previously been reported by our group, and the ICC for the choroidal thickness values between the two observers was very good (from 0.990 to 0.999) [14].

The central sector, the center of the 1.0-mm circle on the ETDRS grid (Figure 2) and the 6×6 rectangular grid (Figure 2) (1×1 mm for each section), was used for the subsequent sector analysis. The 6×6 rectangular grid (36 sections) was divided horizontally into the superior field (18 sections) and inferior field (18 sections). The superior field was divided superiorly inside (including the fovea, eight sections) and outside (the remaining 10 sections), and a similar partition was attempted on the inferior field (Figure 3). This deviation was developed for the present study based on the RNFL lanes.

## Statistical Analysis

We used the JMP, version 10.0.0 software package (SAS Institute Inc., Cary, NC, USA) for the statistical analyses, and the data were expressed as the means ± standard deviation (SD). Values of $p<0.05$ were considered to be statistically significant. For comparisons of the demographic data between the glaucoma and normal subjects, we used Student's *t*-test for the age, IOP and axial length and the chi-square test for sex and the target eye.

We compared the macular choroidal thickness values between the glaucoma patients and normal subjects using an analysis of covariance, with covariance considered for age and the axial length. We used a stepwise regression analysis to evaluate the significant factors affecting the choroidal thickness and the differences in the choroidal thickness values between the sectors in the glaucoma patients based on the following representative factors: age, axial length, CCT and MD. The independent variable criterion of $P = 0.2$ was set for the analysis.

The sample size required to detect a 20% (approximately 40 μm) difference between the glaucoma and normal subjects with a significance level of 5% and a power of 80%, based on the

**Table 3.** The choroidal thickness values in the glaucoma group.

| | mean ±SD | range |
|---|---|---|
| The central sector | 222.6±71.7 | 77.0–397.0 |
| a: superior field ave | 210.4±57.1 | 103.7–346.8 |
| b: inferior field ave | 195.8±54.8 | 88.3–318.6 |
| c: superior inside ave | 202.3±64.1 | 90.0–359.6 |
| d: superior outside ave | 219.8±53.1 | 119.1–332.6 |
| e: inferior inside ave | 190.9±62.6 | 77.6–355.0 |
| f: inferior outside ave | 199.7±50.8 | 96.9–295.4 |
| difference 1 (a-b) | 14.5±29.6 | −55.5–74.8 |
| difference 2 (c-e) | 11.4±24.6 | −45.2–60.1 |
| difference 3 (d-f) | 20.0±33.2 | −64.7–101.8 |

The values are presented as the means±SD (μm).
The values are slightly different from those in Table 2 because these are the raw data.
doi:10.1371/journal.pone.0110265.t003

**Table 4.** The results of symmetrical comparisons between two sectors in the glaucoma group.

| Comparison between two sectors | P value |
|---|---|
| superior vs inferior ave | 0.001 |
| superior inside vs inferior inside ave | <0.001 |
| superior outside vs inferior outside ave | <0.001 |
| superior inside vs outside ave | <0.001 |
| inferior inside vs outside ave | 0.004 |

Ave, average.
All p values were obtained using the paired t-test.
doi:10.1371/journal.pone.0110265.t004

standard deviation of 54.8 μm in the inferior field choroidal thickness average in the glaucoma subjects, was estimated to be 30 patients per group.

## Results

The patient demographics of the two groups and the MD values in the glaucoma patients are shown in Table 1. The glaucoma group consisted of more female patients than the normal group ($P<0.01$). No significant differences were found between the two groups in terms of the age, the target eye, IOP or axial length.

Table 2 shows the results of a comparison of the choroidal thickness values following adjustment for age and the axial length in all sectors, and the p values of the ANCOVA analysis. No significant differences were found between the glaucoma group and the normal group in any sector ($P>0.4$).

The raw data for the choroidal thickness values in the glaucoma group are shown in Table 3, and Table 4 shows a comparison between the superior field sectors and inferior field sectors (symmetrical comparison). The choroidal thickness values were significantly thinner in the inferior sectors in all symmetrical comparisons ($P<0.05$). We also compared the inside and outside choroidal thickness values, and found that the outside choroidal thickness values were significantly thicker in both the superior and inferior fields (all $P<0.05$). These data differ from the values in Table 2 because they were obtained without adjustment for age or the axial length.

### The results of a stepwise regression analysis of independent predictors of the choroidal thickness, and the differences in the choroidal thickness values in all symmetrical sectors among the glaucoma subjects

Table 5 shows the results of the stepwise analyses to determine the predictors of the choroidal thickness using the previously reported factors; age, axial length, CCT and MD. According to these analyses, the age was found to be the most predictive and significant factor for the choroidal thickness in all seven sectors ($P<0.001$). The axial length was the second most predictive factor and was found to be a statistically significant predictor in almost all sectors. The CCT was identified as the only predictive factor in the symmetrical comparisons; however, all adjusted R2 values in the symmetrical comparison were low (0.037–0.063) and were not statistically significant (all $p>0.05$). The MD value was not identified as a significant factor in any sector or in the symmetrical comparisons.

## Discussion

In the present study, we first reported that the whole macular choroidal thickness values in glaucoma subjects do not differ significantly from those of normal subjects. Previous reports have only shown pinpoint measurements of the choroidal thickness obtained using the enhanced-depth imaging method; however, by using SS-OCT, we were able to analyze the whole macular choroidal thickness and compare different sectors. The subjects evaluated in the present study exhibited only focal or diffuse inferior optic rim thinning with corresponding superior visual field damage. We first assumed that in such patients, the inferior macular choroidal thickness might be thinner due to the glaucoma-related damage compared with the superior macular choroidal thickness or the thickness in normal subjects.

However, no significant differences in the macular choroidal thickness were found between glaucoma patients and normal subjects in any of the sectors (All $p>0.4$). Furthermore, our results obtained by a stepwise regression analysis showed that the differences in the choroidal thickness values observed between the superior and inferior sectors had no association with glaucoma damage (MD value), suggesting that the secondary changes due to the progression of glaucoma may not extend to the choroid. This observation was also confirmed by the results of a comparison among sectors in the glaucoma patients (Table 4). The glaucoma patients had thicker values in the superior field than in the inferior field and in the temporal field (outside sector) compared to the nasal field (inside sector) in our study, similar to the findings observed in normal subjects [4,5,18]. The macular choroidal thickness value was affected by age and the axial length, but not the CCT or MD values, according to the stepwise regression analysis performed in this study. Therefore, this result suggests that the whole macular choroidal thickness values of our glaucoma patients were similar to those obtained in normal subjects, as demonstrated in previous reports [5,7,8]. Moreover, the values were not affected by either glaucoma itself or by glaucoma visual field progression.

Both glaucoma patients and normal subjects had a decreased choroidal thickness in inferior sections (Table 2), which is supported by the data form normal adults and children reported by Nagasawa et al. [12]. In addition, the initial changes in glaucoma frequently occur in the inferior optic disc rim, with superior visual field defects being found in glaucoma patients. It has been speculated that inferior choroidal thinning plus some other factors (not choroidal thinning alone) might be associated with the initial glaucomatous changes. However, no mechanism responsible for these changes has been proven. Ikuno et al., advocated two mechanisms underlying the inferior choroidal

**Table 5.** The results of the stepwise regression analyses of the choroidal thickness values using the age, axial length, CCT and MD as variables in the glaucoma group.

| | Independent variables | | | | | | | | | | | |
|---|---|---|---|---|---|---|---|---|---|---|---|---|
| | Age | | | Axial length | | | CCT | | | MD value | | | |
| Dependent variables | Coefficient | F value | P value | Coefficient | F value | P value | Coefficient | F value | P value | Coefficient | F value | P value | Adjusted $R^2$ |
| The central sector | **−4.091** | **17.718** | **<0.001** | **−23.458** | **5.646** | **0.022** | - | | | - | | | 0.287 |
| a: superior field average | **−3.309** | **18.515** | **<0.001** | **−16.963** | **4.715** | **0.036** | - | | | - | | | 0.297 |
| b: inferior field average | **−3.237** | **19.713** | **<0.001** | **−15.246** | **4.239** | **0.046** | - | | | - | | | 0.313 |
| c: superior inside average | **−3.568** | **16.545** | **<0.001** | **−22.536** | **6.369** | **0.015** | - | | | - | | | 0.274 |
| d: superior outside average | **−3.191** | **20.158** | **<0.001** | −13.531 | 3.510 | 0.069 | 0.325 | 1.753 | 0.193 | - | | | 0.318 |
| e: inferior inside average | **−3.418** | **15.629** | **<0.001** | **−21.267** | **5.863** | **0.020** | - | | | - | | | 0.261 |
| f: inferior outside average | **−3.091** | **22.245** | **<0.001** | −10.428 | 2.454 | 0.125 | - | | | - | | | 0.355 |
| Difference 1 (a-b) | - | | | - | | | 0.275 | 3.631 | 0.064 | - | | | 0.063 |
| Difference 2 (c-e) | - | | | - | | | 0.212 | 2.533 | 0.119 | - | | | 0.037 |
| Difference 3 (d-f) | - | | | - | | | 0.329 | 3.395 | 0.073 | - | | | 0.057 |

-: excluded variables.

Statistically significant independent factors for the dependent variables are shown in bold.

doi:10.1371/journal.pone.0110265.t005

thinning in normal subjects; one is the choroidal watershed, which isolates the choroidal circulation, and the other is the fetal choroidal fissure, which closes inferiorly at 16 weeks [19]. It also remains unclear as to why the initial changes due to glaucoma occur in the inferior rim; although gravity may be the simplest explanation.

In a comparison of the group characteristics, our glaucoma patients included more females than the normal control group ($P < 0.01$). This was likely due to patient selection, because typical notches or rim thinning are usually observed in patients with focal ischemic type discs, as classified by Nicolela and Drance [20]. They classified the glaucoma disc morphology into four subtypes: focal ischemic, myopic glaucomatous, senile sclerotic and generalized enlargement. The focal ischemic type is most commonly observed in female patients with primary open angle glaucoma [20], and similar findings have been noted in patients with normal tension glaucoma (NTG) [21].

However, Roberts et al. reported that there was a relationship between these glaucoma optic disc types and the peripapillary choroidal thickness values, in that patients with focal ischemic and generalized enlargement exhibited no statistically significant differences compared to healthy subjects [22]. No significant differences were found in the central sector choroidal thickness between the normal females and males (208.9 μm vs 218.6 μm, $P = 0.678$ by Student's *t*-test). Furthermore, no significant differences were found in the central sector choroidal thickness between female and male glaucoma patients (216.7 μm vs 242.6 μm, $P = 0.347$ according to Student's t-test). These data support our results, and previous reports have shown that sex is not a useful factor for predicting the choroidal thickness [6,8].

Other assessments to clarify the relationship between glaucoma and the choroidal thickness have been carried out by investigating the choroidal thickness values in peripapillary areas [6,22–24]. Because the blood supply of the prelaminar region of the optic nerve head is supplied by peripapillary choroidal vessels, and because the laminar cribrosa is supplied by the arterial circle of Zinn or the branches of the posterior ciliary arteries that supply the choroid [25], investigating the relationship between the peripapillary choroidal thickness and glaucoma is interesting. However, Maul et al. reported that the peripapillary choroidal thickness values were not significantly different between glaucoma and suspected glaucoma patients, and were not associated with glaucoma-related damage or the RNFL thickness [6]. Ehrlich et al. [23]. also reported that the peripapillary choroidal thickness values were not associated with the glaucoma damage, the RNFL thickness or the zone of β clock hours parapapillary choroidal atrophy, which are associated with glaucoma damage [26], in either glaucoma subjects or suspected cases. In addition, Suh et al. used spectral-domain OCT and reported that the peripapillary choroidal thickness values correlated with the subject age and axial length, but not with the CCT, MD, IOP or the presence of systemic disease [24].

These previous reports showed no apparent evidence of a relationship between glaucoma and the peripapillary choroidal thickness, which supports our results showing that neither glaucoma-related visual damage nor glaucoma itself have any apparent associations with the whole macular choroidal thickness.

Meanwhile, Usui et al. hypothesized that the 50% thinning in the choroidal thickness values observed in patients with highly myopic NTG results in reduced choroidal circulation, which may be associated with narrowing of the posterior ciliary arteries due to axial length elongation [11]. The differences in the anatomical structure caused by an abnormal refractive error may account for

the differences in conclusions between the present and that study [11].

One limitation of the present study is that the adjusted $R^2$ values obtained in the stepwise analysis were <0.4. The age and axial length are representative predictive factors for the CT value. However, Aksoy et al. reported that the choroidal thickness is affected by more factors than was previously estimated; for example, the diurnal choroidal thickness changes occur at 30–60 μm, and the use of intravenous acetazolamide increases the CT values [27]. Therefore, we measured the choroidal thickness values during a limited time period (from 1:00 PM to 5:00 PM), and patients receiving an oral topical carbonic inhibitor (acetazolamide) were excluded. However, some patients use topical carbonic inhibitors, which can be absorbed through the mucous membranes in the nose, which then enter the intravenous circulation. In addition, topical prostaglandin analogues and beta blockers have the potential to affect the choroidal thickness. Furthermore, the systolic blood pressure values [16] and hypercholesterolemia [28] may also affect the choroidal thickness; however, these parameters were not examined in this study.

A second limitation is that this study included a relatively small number of subjects. However, it fulfilled a strict power analysis to detect a 20% difference in the choroidal thickness (40 μm) between glaucoma subjects and normal subjects compared with previous reports of 63 μm [5,8]. A third limitation is that whether the choroidal thickness truly represents the choroidal blood flow remains to be elucidated. In healthy younger subjects, the choroidal thickness was not associated with either the total choroidal blood flow or the subfoveal choroidal blood flow [29]. However, systemic administration of sildenafil citrate (Viagra, Pfizer, New York, NY) has been reported to increase the choroidal blood flow and the choroidal thickness in healthy subjects [30]. Further studies are therefore necessary to clarify the relationship between the choroidal thickness and the choroidal blood flow.

The fourth limitation is that we used manual segmentation techniques, according to previous reports. However, Mansouri et al. recently reported that the findings of automated segmentation obtained using SS-OCT are not affected by operator effects, and exhibit a high level of repeatability, and that the main artifact is blinking, not segmentation errors [31]. The fifth limitation associated with this study is that SS-OCT could cover only 20 degrees in the macula area which thus correlated with the first and second test-points in the 30-2 test program. The 10-2 test program was too small for the region and could not reflect the glaucoma visual field damage, therefore the 24-2 test program might closely correlate with the macula area obtained by SS-OCT. In summary, this study demonstrated that neither glaucoma-related visual damage nor glaucoma itself has any apparent association with the whole macular choroidal thickness.

## Supporting Information

**Table S1 The 3D-OCT values in the glaucoma group.** All p values were obtained using the paired t-test. The values are presented as the mean±SD (μm).
(DOCX)

**Data S1**
(XLSX)

## Acknowledgments

The authors thank Hajime Yamakage for his advice on the statistical analyses performed in this study.

## Author Contributions

Conceived and designed the experiments: SN TN HT YK. Performed the experiments: SN TN ET MY. Analyzed the data: SN HT. Contributed reagents/materials/analysis tools: SN. Wrote the paper: SN.

## References

1. Alm A (1992) Ocular circulation. In: Moses R, Hart W (ed.) Adlerã s physiology of the eye; clinical applications.9th ed.St Louis C.V Mosby; 198–227.
2. Leske MC, Heijl A, Hyman L, Bengtsson B, Dong L, et al (2007) Predictors of long-term progression in the early manifest glaucoma trial. Ophthalmology 114(11):1965–1972.
3. Ikuno Y, Kawaguchi K, Nouchi T, Yasuno Y (2010) Choroidal thickness in healthy Japanese subjects. Invest Ophthalmol Vis Sci 51(4):2173–2176.
4. Hirata M, Tsujikawa A, Matsumoto A, Hangai M, Ooto S, et al (2011) Macular choroidal thickness and volume in normal subjects measured by swept-source optical coherence tomography. Invest Ophthalmol Vis Sci 52(8):4971–4978.
5. Mwanza JC, Hochberg JT, Banitt MR, Feuer WJ, Budenz DL (2011) Lack of association between glaucoma and macular choroidal thickness measured with enhanced depth-imaging optical coherence tomography. Invest Ophthalmol Vis Sci 52(6):3430–3435.
6. Maul EA, Friedman DS, Chang DS, Boland MV, Ramulu PY, et al (2011) Choroidal thickness measured by spectral domain optical coherence tomography: factors affecting thickness in glaucoma patients. Ophthalmology 118(8):1571–1579.
7. Rhew JY, Kim YT, Choi KR (2014) Measurement of subfoveal choroidal thickness in normal-tension glaucoma in Korean patients. J Glaucoma 23(1):46–49.
8. Mwanza JC, Sayyad FE, Budenz DL (2012) Choroidal thickness in unilateral advanced glaucoma. Invest Ophthalmol Vis Sci 53(10):6695–6701.
9. Arora KS, Jefferys JL, Maul EA, Quigley HA (2012) The choroid is thicker in angle closure than in open angle and control eyes. Invest Ophthalmol Vis Sci 53(12):7813–7818.
10. Hirooka K, Fujiwara A, Shiragami C, Baba T, Shiraga F (2012) Relationship between progression of visual field damage and choroidal thickness in eyes with normal-tension glaucoma. Clin Experiment Ophthalmol 40(6):576–582.
11. Usui S1, Ikuno Y, Miki A, Matsushita K, Yasuno Y, et al (2012) Evaluation of the choroidal thickness using high-penetration optical coherence tomography with long wavelength in highly myopic normal-tension glaucoma. Am J Ophthalmol 153(1):10–16.
12. Ohno-Matsui K, Akiba M, Moriyama M, Ishibashi T, Tokoro T, et al (2011) Imaging retrobulbar subarachnoid space around optic nerve by swept-source optical coherence tomography in eyes with pathologic myopia. Invest Ophthalmol Vis Sci 52(13):9644–9650.
13. Spaide RF, Akiba M, Ohno-Matsui K (2012) Evaluation of peripapillary intrachoroidal cavitation with swept source and enhanced depth imaging optical coherence tomography. Retina 2012:1037–44.
14. Nagasawa T, Mitamura Y, Katome T, Shinomiya K, Naito T, et al (2013) Macular choroidal thickness and volume in healthy pediatric individuals measured by swept-source optical coherence tomography. Invest Ophthalmol Vis Sci 54(10):7068–7074.
15. Kanamori A, Naka M, Akashi A, Fujihara M, Yamada Y, et al (2013) Cluster analyses of grid-pattern display in macular parameters using optical coherence tomography for glaucoma diagnosis. Invest Ophthalmol Vis Sci 54(9):6401–6408.
16. Usui S, Ikuno Y, Akiba M, Maruko I, Sekiryu T, et al (2012) Circadian changes in subfoveal choroidal thickness and the relationship with circulatory factors in healthy subjects. Invest Ophthalmol Vis Sci 53(4):2300–2307.
17. Tan CS, Ouyang Y, Ruiz H, Sadda SR (2012) Diurnal variation of choroidal thickness in normal, healthy subjects measured by spectral domain optical coherence tomography. Invest Ophthalmol Vis Sci 53(1):261–266.
18. Margolis R, Spaide RF (2009) A pilot study of enhanced depth imaging optical coherence tomography of the choroid in normal eyes. Am J Ophthalmol 147(5):811–815.
19. Ikuno Y, Kawaguchi K, Nouchi T, Yasuno Y (2010) Choroidal thickness in healthy Japanese subjects. Invest Ophthalmol Vis Sci 51(4):2173–2176.
20. Nicolela MT, Drance SM (1996) Various glaucomatous optic nerve appearances: clinical correlations. Ophthalmology 103(4):640–649.
21. Nakazawa T, Shimura M, Ryu M, Himori N, Nitta F, et al (2012) Progression of visual field defects in eyes with different optic disc appearances in patients with normal tension glaucoma. J Glaucoma 21(6):426–430.
22. Roberts KF, Artes PH, O'Leary N, Reis AS, Sharpe GP, et al (2012) Peripapillary choroidal thickness in healthy controls and patients with focal, diffuse, and sclerotic glaucomatous optic disc damage. Arch Ophthalmol 130(8):980–986.
23. Ehrlich JR, Peterson J, Parlitsis G, Kay KY, Kiss S, et al (2011) Peripapillary choroidal thickness in glaucoma measured with optical coherence tomography. Exp Eye Res 92(3):189–194.

24. Suh W, Cho HK, Kee C (2014) Evaluation of peripapillary choroidal thickness in unilateral normal-tension glaucoma. Jpn J Ophthalmol 58(1):62–67.
25. Hayreh SS (1969) Blood supply of the optic nerve head and its role in optic atrophy, glaucoma, and oedema of the optic disc. Br J Ophthalmol 53(11):721–748.
26. Manjunath V, Shah H, Fujimoto JG, Duker JS (2011) Analysis of peripapillary atrophy using spectral domain optical coherence tomography. Ophthalmology 118(3):531–536.
27. Aksoy Y, Çolakoglu K, Kar T, Sevinc MK, Eyi YE (2014) Choroidal thickness is affected by more factors than estimated. Invest Ophthalmol Vis Sci 55(3):1311.
28. Wong IY, Wong RL, Zhao P, Lai WW (2013) Choroidal thickness in relation to hypercholesterolemia on enhanced depth imaging optical coherence tomography. Retina 33(2):423–428.
29. Sogawa K, Nagaoka T, Takahashi A, Tanano I, Tani T, et al (2012) Relationship between choroidal thickness and choroidal circulation in healthy young subjects. Am J Ophthalmol 153(6):1129–1132.
30. Kim DY, Silverman RH, Chan RV, Khanifar AA, Rondeau M, et al (2013) Measurement of choroidal perfusion and thickness following systemic sildenafil (Viagra). Acta Ophthalmol 91(2):183–188.
31. Mansouri K, Medeiros FA, Tatham AJ, Marchase N, Weinreb RN (2014) Evaluation of retinal and choroidal thickness by swept-source optical coherence tomography: repeatability and assessment of artifacts. Am J Ophthalmol 157(5):1022–1032.

PLOS ONE

# Changes in Outer Retinal Microstructures during Six Month Period in Eyes with Acute Zonal Occult Outer Retinopathy-Complex

**Yoshitsugu Matsui[1], Hisashi Matsubara[1], Shinji Ueno[2], Yasuki Ito[2], Hiroko Terasaki[2], Mineo Kondo[1]***

**1** Department of Ophthalmology, Mie University Graduate School of Medicine, Tsu, Japan, **2** Department of Ophthalmology, Nagoya University Graduate School of Medicine, Nagoya, Japan

## Abstract

***Purpose:*** To study the changes in the outer retinal microstructures during a six month period after the onset of acute zonal occult outer retinopathy (AZOOR)-complex by spectral-domain optical coherence tomography (SD-OCT).

***Methods:*** Seventeen eyes of 17 patients with the AZOOR-complex were studied. The integrity of the external limiting membrane (ELM), ellipsoid zone (EZ; also called the inner/outer segment junction), and interdigitation zone (IDZ; also called the cone outer segment tips) were evaluated in the SD-OCT images obtained at the initial visit and at six months. The three highly reflective bands were divided into three types; continuous, discontinuous, and absent. The integrity of the outer nuclear layer (ONL) was also assessed.

***Results:*** Among the three highly reflective bands, the IDZ was most altered at the initial visit and least recovered at six months. Fifteen of 17 eyes (88%) had a recovery of at least one of the three bands at six months in the retinal area where the ONL was intact, and these areas showed an improvement of visual field. Three eyes (18%) had retinal areas where the ONL was absent at the initial visit, and there was no recovery in both the retinal structures and visual fields in these areas.

***Conclusions:*** Our results indicate that more than 85% eyes with AZOOR-complex show some recovery in the microstructures of the outer retina during a six month period if the ONL is intact. We conclude that SD-OCT is a useful method to monitor the changes of the outer retinal microstructure in eyes with the AZOOR-complex.

**Citation:** Matsui Y, Matsubara H, Ueno S, Ito Y, Terasaki H, et al. (2014) Changes in Outer Retinal Microstructures during Six Month Period in Eyes with Acute Zonal Occult Outer Retinopathy-Complex. PLoS ONE 9(10): e110592. doi:10.1371/journal.pone.0110592

**Editor:** Steven Barnes, Dalhousie University, Canada

**Received** May 28, 2014; **Accepted** September 19, 2014; **Published** October 30, 2014

**Copyright:** © 2014 Matsui et al. This is an open-access article distributed under the terms of the Creative Commons Attribution License, which permits unrestricted use, distribution, and reproduction in any medium, provided the original author and source are credited.

**Data Availability:** The authors confirm that all data underlying the findings are fully available without restriction. All relevant data are within the paper.

**Funding:** Grant-in-Aid for Scientific Research C (#20592603) from Ministry of Education, Culture, Sports, Science and Technology (http://www.jsps.go.jp/). The funders had no role in study design, data collection and analysis, decision to publish, or preparation of the manuscript.

**Competing Interests:** The authors have declared that no competing interests exist.

* Email: mineo@clin.medic.mie-u.ac.jp

## Introduction

Acute zonal occult outer retinopathy (AZOOR) is a retinal disease that was first reported by Gass [1]. AZOOR is characterized by an acute loss of one or more zones of outer retinal function, photopsia, minimal funduscopic changes, and electroretinographic (ERG) abnormalities [1–4]. AZOOR occurs predominantly in young women, and some patients have a viral-like illness before the onset [1,4,5]. The exact pathogenesis of AZOOR is still uncertain, but two possible hypotheses have been advanced; virus infection of the photoreceptors [6] and common genetic hypothesis of autoimmune/inflammatory disease [7].

In 2003, Gass suggested that retinal diseases similar to AZOOR, e.g., multiple evanescent white dot syndrome (MEWDS), multifocal choroiditis and panuveitis (MFP), punctate inner choroidopathy (PIC), acute idiopathic blind spot enlargement (AIBSE), acute macular neuroretinopathy (AMN), and AZOOR, were part of a spectrum of a single disease with similar clinical signs, symptoms, and ophthalmological findings [6]. He recommended that these should be placed in a single clinical entity called the AZOOR-complex. There are several studies that reported that two of these diseases can occur in the same patient at the same time or at different times [8–12].

Optical coherence tomography (OCT) is a useful method to detect subtle morphological changes in retinas affected by various pathological conditions. Past studies have demonstrated the diagnostic value of time-domain (TD) and spectral-domain (SD) OCT in eyes with AZOOR-complex. The findings showed that the integrity of the external limiting membrane (ELM), ellipsoid zone (EZ; originally called the inner/outer segment junction [13]) and/or interdigitation zone (IDZ; also called the cone outer segment tips [14]) were disrupted at the retinal areas of visual field defects in eyes with the AZOOR-complex [15–24]. It was also reported that the abnormalities in the outer retinal microstructures can recover during the follow-up period in some patients with the AZOOR-complex [18–20,22]. However, there has not a study that analyzed how these three highly reflective bands change with time during a fixed time period for many patients.

Therefore, the purpose of this study was to determine by SD-OCT the changes in the outer retinal microstructures during a six month period after the initial visit in eyes with AZOOR-complex.

## Subjects and Methods

### Subjects

We reviewed the medical records of patients who were diagnosed with AZOOR-complex who visited the Mie University Hospital or the Nagoya University Hospital from September 2007 to June 2013. Because the purpose of this study was to determine the changes of the retinal microstructures at the early stages of AZOOR-complex, only the patients whose initial examination was ≤3 months from the onset were studied. In addition, only the patients who were followed for at least six months after the initial visit were included. Based on these criteria, seventeen eyes of 17 patients with the AZOOR-complex were studied.

All patients had undergone a complete eye examination including best-corrected visual acuity (BCVA) measured by a standard Japanese decimal visual acuity chart at 5 m, slit-lamp biomicroscopy, color fundus photography, Humphrey static perimetry (30-2 program), and SD-OCT. Fluorescein angiography was performed only at the initial visit. Full-field electroretinograms (ERGs) or multifocal ERGs were recorded at the initial visit for a correct diagnosis of the AZOOR-complex [2,3].

The procedures used conformed to the tenets of the World Medical Association's Declaration of Helsinki. Mie University Institutional Ethics Review Board approved this retrospective study of the patients' medical records. Written informed consent was not given by participants for their clinical records to be used in this study, but patient information was anonymized and de-identified prior to analysis.

### Spectral-domain optical coherence tomography (SD-OCT)

All of the patients had undergone SD-OCT examinations with the Spectralis OCT (HRA+OCT, Heidelberg Engineering) or the Cirrus HD-OCT (version 5.1, Carl Zeiss Meditec). Following the dilation of the pupils, the retinal tomographic images of 9 mm (approximately 30°) horizontal scans for Spectralis or horizontal 6 mm scans for Cirrus were obtained across the fovea. Depending on the image quality, B-scans were averaged.

We evaluated the SD-OCT findings at the initial visit and at six months. The reason why we selected the SD-OCT findings at 6 months was because Gass et al. [4] had reported that the alterations of the patients' vision stabilized within six months of the onset in 77% of the patients. We evaluated the integrity of the three highly reflective bands at the outer retina obtained by the SD-OCT; the external limiting membrane (ELM), ellipsoid zone (EZ) [13], and interdigitation zone (IDZ) [14]. The integrity of these bands was divided into three types; "continuous", "discontinuous", or "absent". The bands were defined as "continuous" when they were seen clearly and appeared to be continuous. The bands were defined as being "discontinuous" when they were blurred or interrupted. The bands were defined as "absent" when they were not identified at the area of the visual field defect. These decisions were made by two retinal specialists (YM and HM) independently and were masked to the other clinical findings. In addition, the preservation of outer nuclear layer (ONL) was also assessed.

To evaluate the changes in the outer retinal highly reflective bands more quantitatively, a longitudinal reflectivity profile (LRP) was created by previously described methods [13,25,26]. In brief, one vertical straight line was drawn at the retinal area of the visual field defect. The LRPs were made by calculating median values of pixels across each level of 20 adjacent A-scans using ImageJ (National Institutes of Health, Bethesda, MA; available at rsbweb.nih.gov/ij/download.html).

## Results

The clinical characteristics and SD-OCT findings of the 17 Japanese patients with AZOOR-complex (three men and 14 women; age, 19–49 years) are summarized in Table 1. The diagnosis of our 17 patients included 10 with AZOOR, 4 with MEWDS, and 3 with AIBSE. The average interval between the onset of symptoms and examination in our hospital was 3.6 weeks with a range of 1 to 12 weeks. The average spherical equivalent refractive error was -4.4 diopters (D) with a range of -0.5 to -13.5 D. The type of visual field defects included two with a central scotoma, six with a paracentral scotoma, two with a temporal scotoma, and seven with a centro-temporal scotoma (Table 1).

### Case Presentations

**Case 11: MEWDS Associated with ONL Loss.** A 35-year-old myopic woman presented with complaints of acute vision reduction and photopsia in her right eye. Her decimal best-corrected visual acuity (BCVA) was 0.5 OD, and perimetry showed a visual field defect within 30 degrees of the fovea (Fig. 1A). Fundus examination showed multiple small, gray-white patches at the level of RPE and outer retina in the mid-peripheral region, and these white patches disappeared within four weeks without treatment. Based on these clinical findings, she was diagnosed with MEWDS. She was followed up without any treatments.

Her SD-OCT findings at the initial visit are shown in Figures 1B and 1C. In the central retinal area where the ONL was intact (yellow dotted square, Fig. 1B), the ELM was judged to be "discontinuous", and the EZ and IDZ were classified as being "absent". This was because these two lines were merged with the RPE-Bruch's membrane complex and were not identified as independent bands (Fig. 1C).

At six months after the initial visit, the decimal BCVA had improved to 1.2, and the visual field had recovered at many points (Fig. 1D). SD-OCT also showed an improvement in the outer retinal microstructures but only at the area of the intact ONL (yellow dotted square, Figs. 1E and 1F). At this time, the ELM and EZ were judged as "continuous", but the IDZ was still judged as "discontinuous" at the central area.

We also noted that this patient had an area of the retina where the ONL was completely absent at the initial visit (red square, Fig. 1B), and there was no recovery of the both the visual field and the SD-OCT image in this area at 6 months (red square, Fig. 1E).

**Case 1: AZOOR with Recovery of Outer Retinal Microstructures.** A 30-year-old emmetropic woman had an acute onset of photopsia and vision reduction in her right eye. Her decimal BCVA was 1.0 OD, and fundus examination and fluorescein angiography were essentially normal. However, perimetry showed severely decreased retinal sensitivities within 20 degrees of the fovea in the right eye (Fig. 2A). Multifocal ERGs also showed reduced focal ERGs within 20 degrees of the fovea. Based on these findings, this patient was diagnosed with AZOOR. She was followed without any treatments.

Her SD-OCT findings at the initial visit are shown in Figures 2B and 2C. The ELM and EZ were judged to be "discontinuous", because they were disrupted away from the macula (Figs. 2B and 2C). The IDZ was judged to be "absent" because this band was not identified over the entire 9 mm scan.

**Table 1.** Clinical Characteristics and SD-OCT findings of Patients with AZOOR-Complex.

| Case/Sex/Age (y)/Eye | Diagnosis | Initial visit from the onset (week) | Spherical equivalent refractive error (dioptor) | Type of Scotoma | BCVA initial/6M | ELM initial/6M | EZ initial/6M | IDZ initial/6M | Improvement in visual field |
|---|---|---|---|---|---|---|---|---|---|
| 1/F/30/Right | AZOOR | 2 | −0.5 | Paracentral | 1.0/1.2 | II/I | II/I | III/II | Significant |
| 2/M/35/Right | AZOOR | 4 | −0.5 | Paracentral | 1.2/1.5 | I/I | I/I | II/I | Significant |
| 3/F/34/Right | AZOOR | 1 | −11.5 | Centro-temporal | 0.5/0.7 | II/II | III/III | III/III | None |
| 4/F/19/Right | AZOOR | 2 | −3.0 | Temporal | 0.9/1.2 | II/I | II/I | III/III | Mild |
| 5/F/49/Left | AZOOR | 12 | −13.5 | Centro-temporal | 0.8/0.6 | III/III | III/III | III/III | None |
| 6/F/30/Right | AZOOR | 4 | −7.0 | Centro-temporal | 0.5/0.8 | I/I | II/I | II/III | Mild |
| 7/F/37/Left | AZOOR | 1 | −8.5 | Centro-temporal | 0.6/1.0 | II/I | II/I | III/III | Mild |
| 8/F/25/Left | AZOOR | 8 | −6.6 | Centro-temporal | 0.2/0.8 | I/I | II/I | III/III | Mild |
| 9/M/42/Right | AZOOR | 2 | −6.0 | Paracentral | 1.2/1.2 | I/I | II/I | III/II | Mild |
| 10/F/19/Right | AZOOR | 1 | −4.5 | Centro-temporal | 0.6/1.2 | II/II | II/I | III/II | Significant |
| 11/F/35/Right | MEWDS | 2 | −10.0 | Central | 0.5/1.2 | II/I | III/I | III/II | Significant |
| 12/F/31/Left | MEWDS | 1 | −6.5 | Central | 0.3/1.2 | II/I | II/I | III/I | Significant |
| 13/M/39/Right | MEWDS | 8 | −0.5 | Centro-temporal | 0.2/1.2 | II/I | III/I | III/II | Significant |
| 14/F/24/Right | MEWDS | 1 | −2.75 | Paracentral | 0.8/1.2 | II/I | II/I | III/II | Significant |
| 15/F/47/Right | AIBSE | 1 | −2.0 | Temporal | 1.2/1.2 | I/I | II/I | III/III | None |
| 16/F/37/Left | AIBES | 3 | −0.5 | Paracentral | 1.2/1.0 | II/I | II/I | III/I | Significant |
| 17/F/29/Left | AIBSE | 8 | −5.75 | Paracentral | 1.0/1.2 | I/I | II/I | III/II | Significant |

Abbreviations: AZOOR, acute zonal occult outer retinopathy; MEWDS, multiple evanescent white dot syndrome; AIBSE, acute idiopathic blind spot enlargement; BCVA, best-corrected visual acuity; ELM, external limiting membrane; EZ, ellipsoid zone; IDZ, interdigitation zone; I, continuous; II, discontinuous; III, absent.

doi:10.1371/journal.pone.0110592.t001

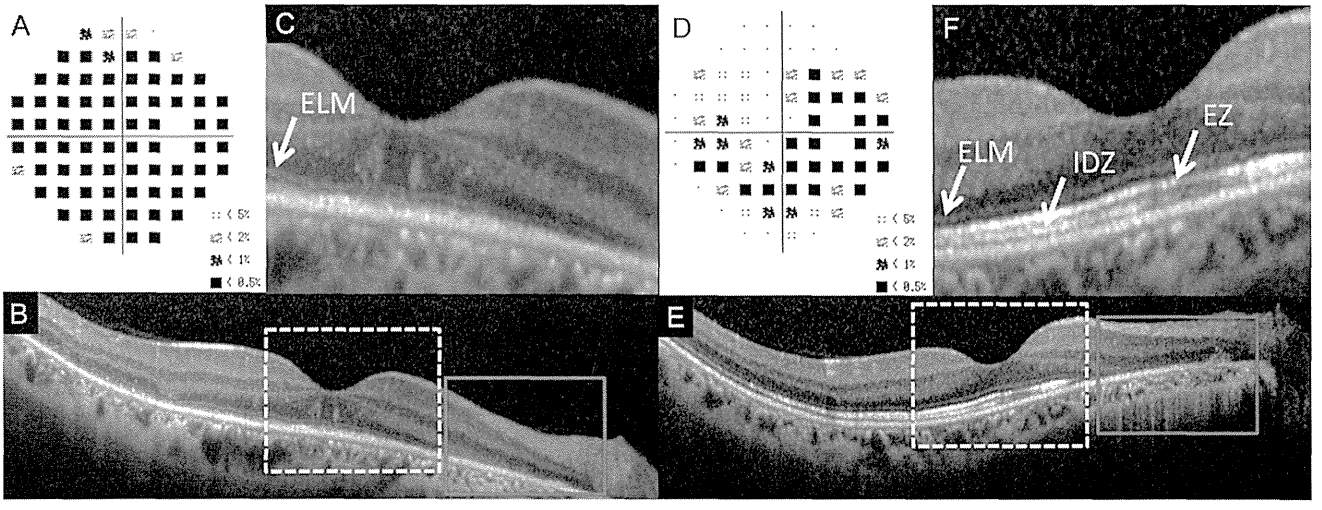


**Figure 1. Static visual field and spectral-domain optical coherence tomographic (SD-OCT) results of the right eye of Case 11 at the initial visit (A–C) and six months after the initial visit (D–F).** A: Deviation plot obtained by the Humphrey 30-2 program at the initial visit. B: Horizontal SD-OCT image through the fovea at the initial visit. C: Magnified view of the area outlined by dashed yellow line box in the image of B. D: Deviation plot obtained with the Humphrey 30-2 program at six months after the initial visit. E: Horizontal SD-OCT image through the fovea at six months after the initial visit. F: Magnified view of the area outlined by dashed yellow line box in the image of E. ELM, external limiting membrane. EZ, ellipsoid zone. IDZ, interdigitation zone. This case had the retinal area where the outer nuclear layer (ONL) was completely absent (red line boxes).
doi:10.1371/journal.pone.0110592.g001

Interestingly, the retina had highly reflective materials in columns which passed through the ONL from the RPE at the area of visual field defect (red arrows, Fig. 2C). Similar highly reflective materials have been reported in a patient with MEWDS [20].

After six months, there was a marked improvement in her visual fields (Fig. 2D), and SD-OCT showed a recovery of the outer retinal microstructures. At this time, the ELM and EZ were judged to be "continuous". However, the IDZ was still "discontinuous", because it was only identified in the central area (Figs. 2E and 2F). We also noticed that the columnar highly reflective materials were not present at six months. The ONL was preserved in the initial and 6 months SD-OCT images.

**Case 2: AZOOR with Intact EZ at Initial Visit.** A 35-year-old healthy emmetropic man reported that he had an acute paracentral visual field depression and photopsia in his right eye. His decimal BCVA was 1.2 OD. His fundus and fluorescein angiography were normal, but visual field showed extensive defects outside the fovea in the right eye (Fig. 3A). His scotopic and photopic full-field ERGs were reduced but only in the right eye.

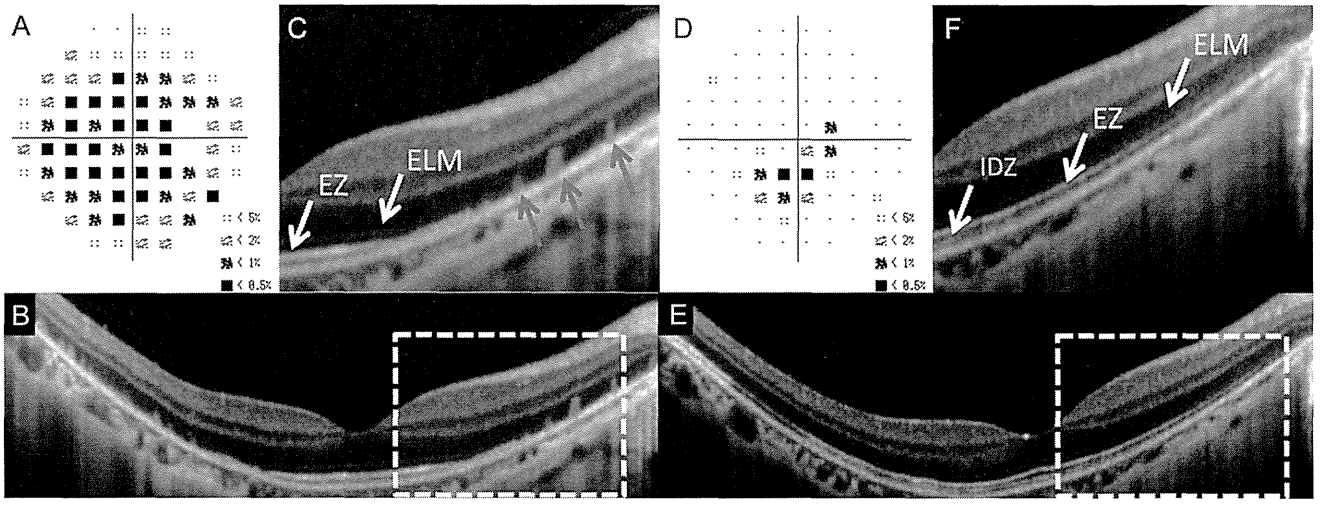


**Figure 2. Static visual field and spectral-domain optical coherence tomography (SD-OCT) results of the right eye of Case 1 at the initial visit (A–C) and six months after the initial visit (D–F).** A: Deviation plot obtained with the Humphrey 30-2 program at the initial visit. B: Horizontal SD-OCT image through the fovea at the initial visit. C: Magnified view of the area outlined by dashed yellow line box in B. D: Deviation plot obtained with the Humphrey 30-2 program at six months after the initial visit. E: Horizontal SD-OCT image through the fovea at six months after the initial visit. F: Magnified view of the area outlined by dashed yellow line box in the image of B. ELM, external limiting membrane. EZ, ellipsoid zone. IDZ, interdigitation zone. Several column-shaped highly reflective materials are seen at the outer retinal area of visual field defect at the initial visit (red arrows).
doi:10.1371/journal.pone.0110592.g002

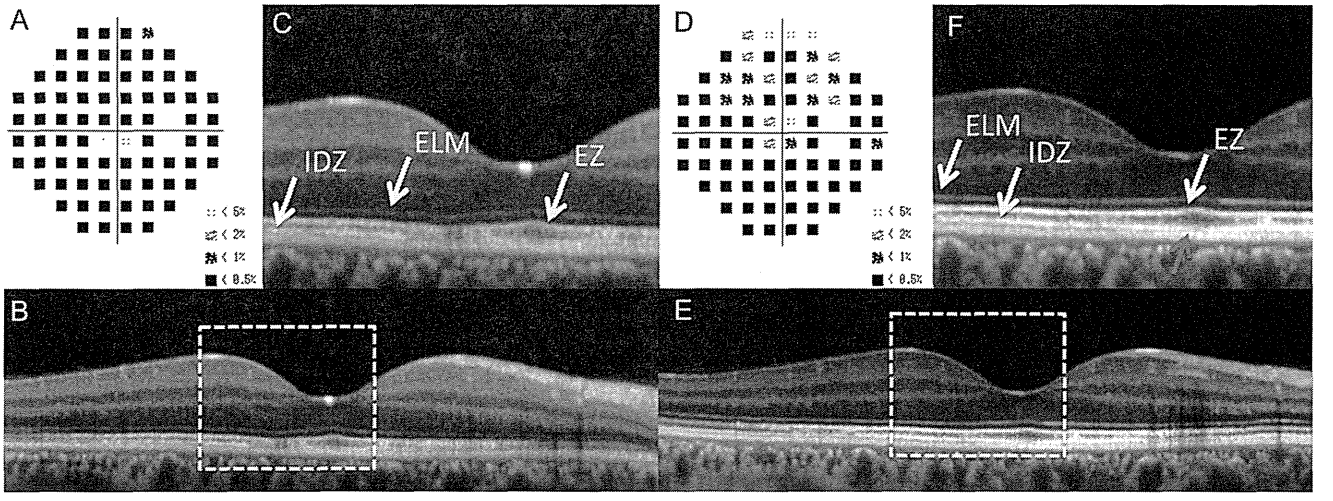


**Figure 3. Static visual field and spectral-domain optical coherence tomographic (SD-OCT) results in the right eye of Case 2 at the initial visit (A–C) and six months after the initial visit (D–F).** A: Deviation plot obtained with the Humphrey 30-2 program at the initial visit. B: Horizontal SD-OCT image through the fovea at the initial visit. C: Magnified view of the area outlined by dashed yellow line box in the image of B. D: Deviation plot obtained by the Humphrey 30-2 program at six months after the initial visit. E: Horizontal SD-OCT image through the fovea at six months after the initial visit. F: Magnified view of the area outlined by dashed yellow line box in the image of B. The COST line is still blurred near the fovea (red arrow). ELM, external limiting membrane. EZ, ellipsoid zone. IDZ, interdigitation zone.
doi:10.1371/journal.pone.0110592.g003

Based on these findings, he was diagnosed with AZOOR. He was treated with intravenous drip methylprednisolone.

His SD-OCT findings at the initial visit are shown in Figures 3B and 3C. The ELM and EZ were judged to be "continuous", but the IDZ was judged to be "discontinuous" (Fig. 3B & 3C).

Six months later, he reported some improvements of his visual symptoms, and his visual field showed recovery at several points (Fig. 3D). At this time, the ELM and EZ were judged to be "continuous", but the IDZ was judged to be "discontinuous", because it was still blurred near the fovea (yellow arrow, Fig. 3F, red arrow). The ONL was intact both at the initial visit and at 6 months.

To evaluate the changes in outer retinal high-reflective bands more quantitatively, a longitudinal reflectivity profile (LRP) was created in the retina of Case 2 (Fig. 4). One vertical straight line was drawn at 0.5 mm temporal retina from the foveola (red dotted lines of Fig. 4). We found that that IDZ was undetectable at the initial visit, but it became detectable as a third highly reflective band six month later (Figs. 4C and 4E).

**Case 3: AZOOR with Worsening of Visual Fields.** A 34-year-old myopic woman reported experiencing photophobia and vision reduction of one month duration in her right eye. She had a history of Basedow disease for eight years. Her decimal BCVA was 0.5 OD. Fundus examination and fluorescein angiography were normal, but Humphrey visual field tests revealed a temporal scotoma extending into the fixation point in the right eye (Fig. 5A). The multifocal ERGs were reduced in the centro-temporal field. Based on these clinical findings, she was diagnosed with AZOOR. She was treated with intravenous drip methylprednisolone.

Her SD-OCT findings of the right eye at the initial visit are shown in Figures 5B and 5C. Her ELM and EZ were judged to be "discontinuous", and the IDZ was judged to be "absent". Despite intravenous drip methylprednisolone and following orally administrated predonisolone for six months, she felt that there was a gradual worsening of her visual decrease, and visual field tests showed an enlargement of the temporal scotoma (Fig. 5D). At this time, the ELM and EZ were judged to be "discontinuous", and the IDZ still remained "absent" (Figs. 5E and 5F). The ONL thickness was also reduced at the areas of the visual field defects.

### Summary of SD-OCT findings

The changes in the ELM, EZ, and IDZ at the initial visit and six months later are summarized in Figure 6 (see also Table 1). The status of the three highly reflective bands were evaluated at the retinal areas with visual field defects. In this evaluation, we excluded the retinal areas of undetectable ONL, because we noted that the retinal areas with loss of ONL at the initial visit did not show any improvement both in the SD-OCT findings and the visual field defects. Therefore in Figure 6, the results are shown only at the retinal areas of intact ONL.

We found that the IDZ was most vulnerable among the three outer retinal bands at the initial visit. There were no AZOOR-complex patients who had a continuous IDZ at the area of visual field defect at the initial visit. The IDZ was also most slow to recover at six months after the initial visit. Even at six months, the IDZ was continuous only in three eyes (18%), discontinuous in six eyes (35%), and still absent in eight eyes (47%).

When compared to the IDZ, the ELM and EZ were relatively well preserved at six months. The ELM was continuous in 14 of 17 eyes (82%) at six months. Similarly, the EZ was continuous in 15 of 17 eyes (88%) at six months (Fig. 5).

We also found that 15 of 17 eyes (88.3%) had a recovery of at least one of the three bands during six months (Table 1) if the ONL was intact, and these 15 eyes also showed an improvement of the visual field defects.

## Discussion

We investigated the changes in the outer retinal microstructures at the initial visit and six months later in 17 eyes with AZOOR-complex using the SD-OCT. There have been many case series which described the change of OCT findings with time in AZOOR-complex patients [12,15–24], but the best of our knowledge, this is the first systematic report focusing on the

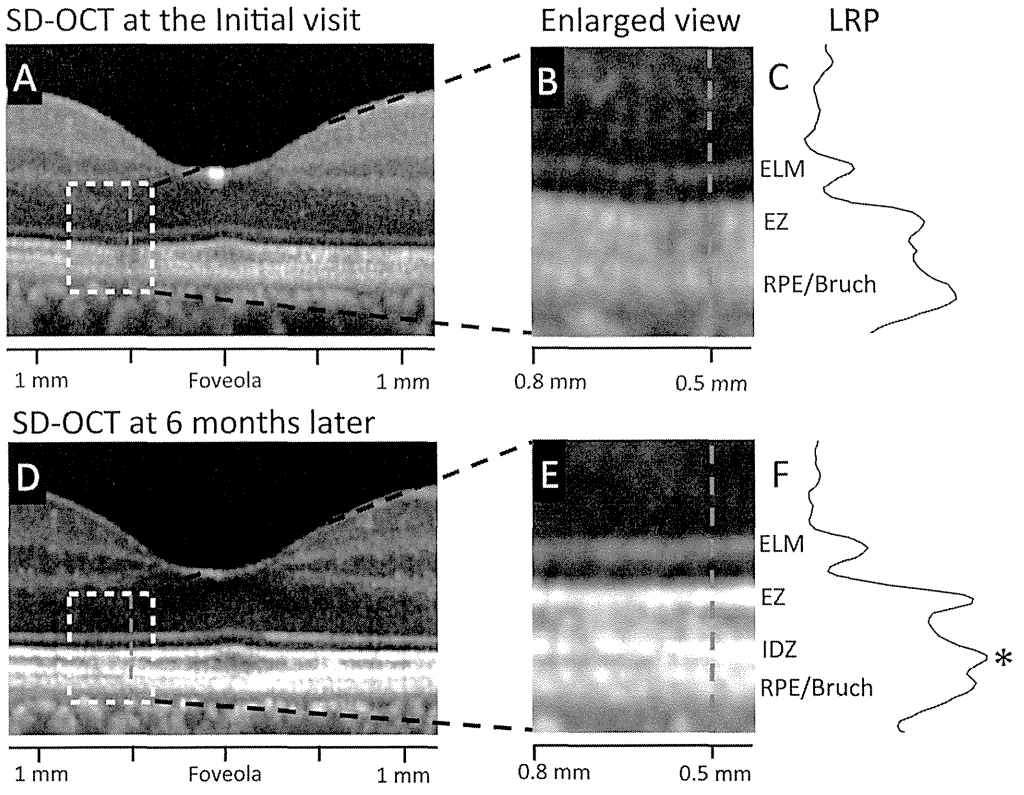


**Figure 4. Results of longitudinal reflectivity profile (LRP) in the retina of Case 2.** A. Horizontal SD-OCT scan through the fovea at the initial visit. B. Magnified view of the area outlined by dashed white line box in the image of A. C. Longitudinal reflectivity profile (LRP) along the vertical line at 0.5 mm temporal from the foveola (red dotted line) at the initial visit. D. Horizontal SD-OCT scan through the fovea at six months after the initial visit. E. Magnified view of the area outlined by dashed white line box in the image of D at six months after the initial visit. F. Longitudinal reflectivity profile (LRP) along the vertical line at 0.5 mm temporal from the foveola (red dotted line) at six months after the initial visit. At the retinal area of 0.5 mm temporal from the foveola, IDZ was nearly undetectable at the initial visit, but the peak of IDZ was clearly detectable as a third highly reflective band at six month later (asterisk). ELM, external limiting membrane. EZ, ellipsoid zone. IDZ, interdigitation zone. RPE/Bruch, retinal pigment epithelium/Bruch's membrane complex. LRP, longitudinal reflectivity profile.
doi:10.1371/journal.pone.0110592.g004

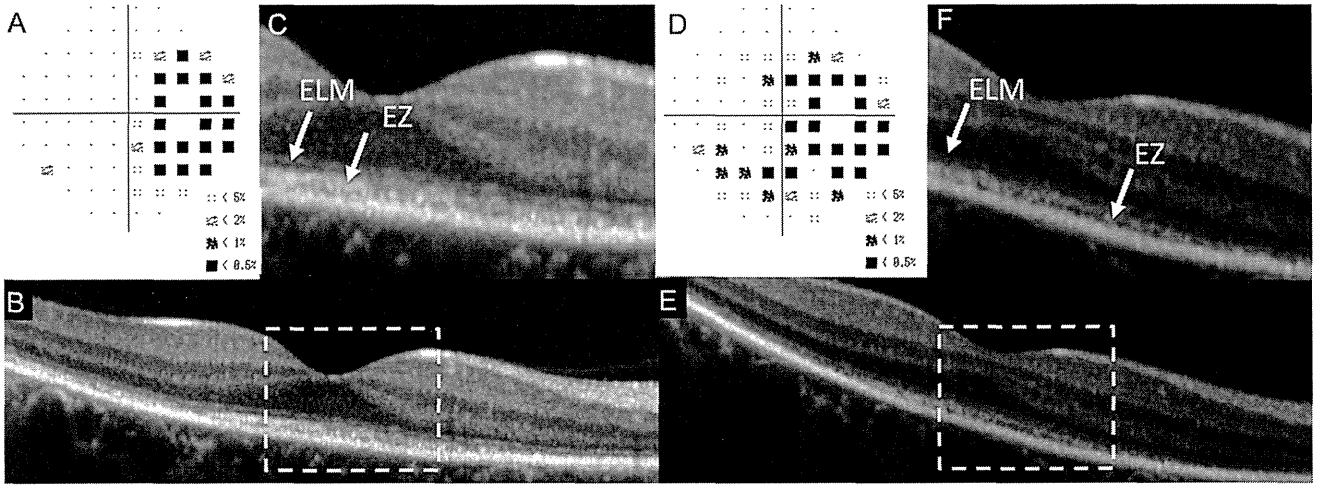


**Figure 5. Static visual field and spectral-domain optical coherence tomographic (SD-OCT) results in the right eye of Case 3 at the initial visit (A–C) and six months after the initial visit (D–F).** A: Deviation plot obtained by the Humphrey 30-2 program at the initial visit. B: Horizontal SD-OCT image through the fovea at the initial visit. C: Magnified view of the area outlined by dashed yellow line box in the image of B. D: Deviation plot obtained by the Humphrey 30-2 program at six months after the initial visit. E: Horizontal SD-OCT image through the fovea at six months after the initial visit. F: Magnified view of the area outlined by dashed yellow line box in the image of E. ELM, external limiting membrane. EZ, ellipsoid zone. IDZ, interdigitation zone.
doi:10.1371/journal.pone.0110592.g005